universität wien

MASTERARBEIT / MASTER'S THESIS

Titel der Masterarbeit / Title of the Master's Thesis

„A Model of Motion of Autophagosomes“

verfasst von / submitted by

Don Ciglenečki, BSc

angestrebter akademischer Grad / in partial fulfilment of the requirements for the degree of

Master of Science (MSc)

Wien, 2018 / Vienna 2018

Studienkennzahl lt. Studienblatt / degree programme code as it appears on the student record sheet:	A 066 824
Studienrichtung lt. Studienblatt / degree programme as it appears on the student record sheet:	Masterstudium Mathematik UG2002
Betreut von / Supervisor:	Univ.-Prof. Dr. Christian Schmeiser

Abstract

The autophagy is a biological process during which an autophagosome moves through the cell until it attaches to the vacuole. Due to technical limitations, the motion can not be observed directly; only the initial and final position of the autophagosome can be located by microscope. The aim of this thesis is to determine whether the type of motion can be specified from the probability distribution of the final location alone.

The motion has been modeled consisting from two components; diffusion and advection. A simplified 2-dimensional model has been used to examine the behavior of the theoretical case of infinite advection combined with infinitely small absorption on the vacuole. The 3-dimensional model has been analyzed by numerical methods. Effects of different parameter choices has been compared in order to specify whether they can be uniquely determined from the final distribution along the vacuole.

Zusammenfassung

Die Autophagie ist ein biologischer Prozess, bei dem sich ein Autophagosom durch die Zelle bewegt bis es sich an die Vakuole befestigt. Aufgrund technischer Einschränkungen kann die Bewegung nicht direkt beobachtet werden; nur die Anfangs- und Endposition des Autophagosomes kann man mit dem Mikroskop lokalisieren. Das Ziel dieser Arbeit ist es zu bestimmen, ob die Art der Bewegung allein aus Wahrscheinlichkeitsverteilung der Endposition auf der Vakuole bestimmt werden kann.

Das verwendete Model der Bewegung besteht aus zwei Komponenten; Diffusion und Advektion. Ein vereinfachtes zweidimensionales Modell wurde verwendet, um das Verhalten des theoretischen Falles der unendlichen Advektion kombiniert mit einer unendlich kleinen Absorption entlang der Vakuole zu untersuchen. Das 3-dimensionale Modell wurde mit numerischen Methoden analysiert. Die Auswirkungen verschiedener Parametergrößen wurden verglichen, um zu bestimmen, ob die Parameter aus der endgültigen Verteilung entlang der Vakuole eindeutig bestimmt werden können.

Acknowledgements

I would like to express gratitude to my supervisor, Prof. Christian Schmeiser for his extensive and helpful support .

Further, I would to thank Daniel Papinski from Max. F. Perutz Laboratories in Vienna. The thesis is wholly centered on the experiment he made.

Especially, I would like to thank to my family for their support through the duration of my studies.

Contents

1 Introduction

[1] The term "autophagy" derives from its Greek meaning ("self-devouring") and denotes a self-degradative process, where (mostly) unnecessary or dysfunctional components of the cell will be disassembled and possibly reused as nutrients for the cell.

The autophagy intensifies in the periods of starvation and helps to provide nutrients for the cell during critical times. It also helps the cell to remove potentially harmful objects, such as misfolded or aggregated proteins, damaged organelles or intracellular pathogens. Moreover, in some cases autophagy promotes cellular senescence (i.e. aging of the cell), which prevents cells from dividing infinitely. Together with some other effects, this gives the autophagy an important role in prevention of diseases such as cancer, neurodegeneration and many more.

The autophagy is a comparably new field of research. At the morphological level it was described already in 1950s, but only in the last two decades the researchers began to get insight in the underlying molecular and biological mechanisms.

An important open question remains, which of the intracellular mechanisms are responsible for the transport of the material to the site where it should be disassembled. Many experiments have been conducted, like the ones in [3], using reagents to neutralize some of the intracellular structures and inspecting the impact on the autophagic process.

This thesis is centered on the experiment done by Daniel Papinski from Max. F. Perutz Laboratories in Vienna. In contrast to those mentioned before, his experiment is based solely on observations by microscope. The aim of the thesis is to construct a mathematical model of motion, which should provide a possible explanation for the numerical results of the experiment.

2 Structure of the Thesis

- In the section 3, the biological background is represented in extent necessary for the later work.
- The section 4 contains the details about the experiment.
- In the section 5 the methods of mathematical modeling are explained and applied to construct the framework of the model
- In the section 6, an extreme case of infinite advection velocity and infinitely small absorption will be discussed using analytical methods.
- In the section 7, the model will be analyzed by numerical means.
- The section 8 deals with the question whether the searched parameters can be derived from results in the previous sections.
- In the section 9 the results will be summarized.
- The Appendix contains the program code used for the numerical computations.

[1] Biological basics presented in this section are mostly taken out of [1] and [2].

3 Biological Background

This section summarizes the biological conditions on which later the mathematical model will be constructed. In 3.1, the geometric environment of the cell will be introduced, while in the subsequent subsections the process of autophagy will be explained. The exact chemical and biological structure underlying the autophagy is not yet discovered; after all the aim of the experiment is to improve the knowledge about it. Therefore, in 3.3 and 3.4, different possible scenarios will be compared and the differences in characteristics, which could possibly influence the outcome of the experiment will be highlighted.

3.1 Structure of the cell

The autophagy is an intracellular process, therefore a single cell will represent the entire environment of our model. The experiment will be conducted on a yeast cell. [2]

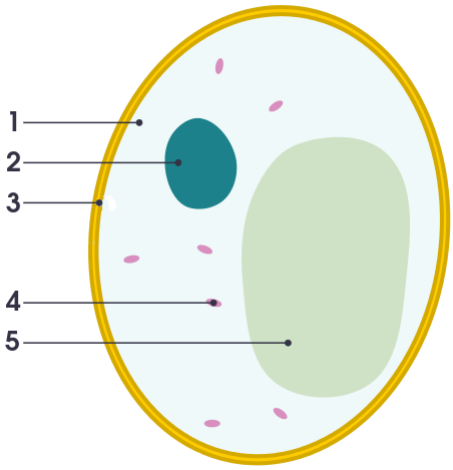

Figure 1: Basic components of a yeast cell:
(1) Cytoplasm consists of fluid called cytosol, small organelles and cytoskeleton inside it
(2) Nucleus is responsible for the storage and processing of DNA. Important for our model: It is surrounded with it's own membrane, therefore the cytosol cannot flow through this area.
(3) Cell membrane prevents fluid from leaving the cell
(4) Mitochondria are much smaller than nucleus, but they are also surrounded with their own membrane and impassable for most objects or fluids.
(5) Vacuole is an enclosed compartment mainly filled with water. It serves as a storage for different substances.

3.2 Autophagy; the Structure of the Process

[3] There are various types of autophagy; most notably the micro-autophagy, where the vacuolar membrane will directly absorb nearby cargo and the macro-autophagy, where the cargo will be delivered to the vacuole from more distant parts of the cell. This thesis refers entirely to the macro-autophagy (autophagy in the following). The latter can be described roughly divided in three steps:

1. Lipid bilayer membrane known as phagosphore expands to engulf the cargo (i.e. the material which should be disassembled) and forms a vesicle around it. Such vesicle is called autophagosome.

2. The autophagosome will be delivered from it's initial position to the vacuole (or to lyzosome in some cells). It is not known which mechanism underlies this motion. This step is the topic of our research.

[2] The graphics is taken from [5]. The explanations on the right side are summarized from [7] and [8]
[3] The content of this section originates from [1], [2] and [12].

3. The autophagosome fuses with the vacuole and releases the cargo to its interior, where it will be disassembled.

3.3 Random and Controlled Processes

Physical processes and chemical reactions involved in the autophagy can occur randomly or under supervision of some signaling mechanism controlling each (or some) step(s) of the process. Combining random and deterministic components will have an important role in the construction of the mathematical model later.

An important example is the classification of the autophagy with respect to the step of the autophagosome formation (step 1 in the above subsection):

- Non-selective autophagy: Here the cargo determined for the decomposition will be selected randomly.
- Selective autophagy: Here some specific intracellular structure will be targeted and taken as cargo. Thereby the damage on the cell structure can be omitted. Moreover, the cell can use this mechanism to eliminate unwanted structures.

We encounter a similar situation at the step 2 from the above subsection; the movement of the autophagosomes can be either

- directed motion driven by some specified intracellular mechanism.
- nondirected motion driven by fluid diffusion and/or different nonspecified mechanisms.

In many articles about autophagy, like [3] and [1], the authors discuss the possible role of the cytoskeleton in the controlling mechanism needed for the selective autophagy and try to prove, whether the disruptions of the cytoskeleton network affect the intensity of the autophagic process. The involvement of the cytoskeleton in the autophagic process as a whole suggests that it could also play a role in the movement of the autophagosomes. As described in the following subsection, the structure of the cytoskeleton is known to drive the motion in many other cellular processes.

3.4 The Cytoskeleton

The cytoskeleton is a network of elongated protein polymer fibers that support cell shape, compartmentalization and movements of components inside the cell or even whole-cell movement.

Analogously to the researches described in [3] and [1], here I will focus on two components of the cytoskeleton, namely on filaments made of polymerized tubulin called the microtubuli and on the actin filaments.

Filaments of the cytoskeleton form a complex network, which can serve as tracks for intracellular movement powered by specific motor proteins. Kinesins move cargo along the microtubuli towards their plus ends, whereas dyneins enable the movement towards the minus ends of the microtubuli. In a similar way myosins enable movement along the actin filaments.

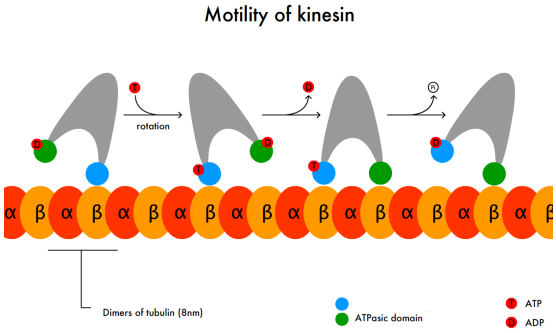

[6]

1. Microtuboli Microtuboles are highly dinamic tube-like structures formed by polymerization of dimers of α and β tubolin. Because of the arrangement of the tubulin dimers within the microtubule, α-tubulins are exposed at one end while β-tubulins are exposed at the other. This gives the microtubule a structural polarity; equivalently, it forms a tube with a plus and a minus end. The minus ends are anchored near the center of the cell to the microtubule organizing center, whereas the plus ends extend towards the cell surface.

   The role of microtubules in autophagy is still an open issue. Kirisako et al. (1999) revealed that treatment of yeast cells with nocodazole, a chemical which disrupts microtubules, doesn't affect autophagy, which gives the impression that in this case the microtubules are not involved in the autophagy. [1]

   On the other hand, some studies dealing with other types of cells have come to different results. Fass et al. (2006) investigated the mammalian cells, where the autophagosomes target the lyzosomes. They claim that phagosphores do not move along the microtubuli, but mature autophagosomes do. Using time-lapse video microscopy in 10s intervals, they concluded that a typical autophagosome demonstrates long distance, rapid directional movements of about 0.3 μm/s period, followed by short, random movements or pauses. After application of nocodazole the long directional movements vanished. However, measures show that this does not affect the life span of the autophagosomes or their fusion with lysosomes. Therefore, the microtubule-dependent movement is in this case dispensable for autophagy. This may arise from the fact that upon microtubule depolymerization the tight association that exists between lysosomes and microtubules is disrupted, and lysosomes become distributed throughout the cytoplasm. [4]

   The microtubules are nucleated at organelles called microtubule organizing centers. As they often stay pointing towards the respective microtubuli organizing center with one of their ends, this leads them to have to some extent centrally ordered spatial distribution.

2. Actin network Actin filaments are again polarized tube-like structures supporting the cell shape, which differ from the microtubuli i.a. in the following: (from [1])

   - Diameter and the length of actin filaments is significantly shorter.
   - Their spatial orientation is more random.
   - Branching is possible; if Arp 2/3 complex binds on the side of an existing filament, then a formation of a new filament begins at the angle of 70° relative to the existing filament.

   At least two different studies claim that blocking the actin polymerization does not affect the bulk/nonselective autophagy in the yeast. To the contrary, some studies (listed in [1]) show that actin filaments are needed for the selective type of autophagy.

In both cases, the studies deal with the question, whether the cargo can be successfully delivered to the corresponding destination after blocking the actin network by some chemical reagent. This does not necessary explain, whether the exact route of the autophagosome movement is influenced by moving along the actin network or not. For example, in [3] the authors studied the cytoplasm to vacuole targeting pathway (Cvt), a process which is closely related to selective type of autophagy. They showed, that after blocking the actin network, the cargo won't be properly recognized and packed into Cvt vesicles (the Cvt equivalent of the autophagosomes). This defect is caused by an inability to recruit the Cvt complex to the pre-autophagosomal structure in the absence of actin cables.

Summarizing the above, the experiments conducted by disrupting the microtubuli or actin network using some chemical reagent show that these two networks have a role at least in some types of autophagy. However, both are or could be included already in the early stages before the autophagosomes are formed. It is therefore not always possible to conclude from this experiments, whether the mature autophagosomes move along the microtubuli or actin network. Moreover, using such reagents can damage the components of the cell other than microtubuli or actin and thereby influence the results.

4 The Experiment

The interior of the yeast cells has been photographed with an inverted microscope[4]. The technology used allows to photograph 2-dimensional slices through the cell. Slices of 240 nm has been chosen to cover the whole cell. About 100 ms have been necessary to scan a single slice.

Due to long time necessary to cover the whole cell, it was not possible to track the position of the cargo directly during the motion. Instead only two images has been taken during each repetition of the experiment;

1. one displaying the cell with the cargo on the initial position and
2. one displaying the cell with the cargo attached to the vacuole.

The images has been taken approximately in time distance of about 20 minutes.

By repeating the procedure described above sufficient times, the probability density of the final cargo location on the vacuole can be computed.

Definition 1 ${}^{e}\rho_{\infty}(x)$ *denotes the probability density of the final cargo location on the vacuole as measured during the experiment.*

The location on the vacuole x can be given by Cartesian coordinates or by an angle as it will be defined later. In the following it will be assumed that ${}^{e}\rho_{\infty}$ is the only new information obtained from the experiment.

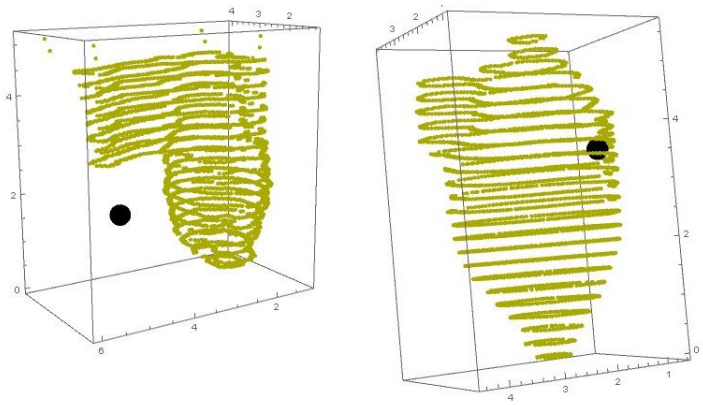

Figure 2: An examples of data from the experiment. The vacoule is represented with green dots. Slices are clearly visible. The black dot is the cargo. Left: before the motion Right: after the motion.

[4]The microscope was an Olympus IX-83 with an OrcaFLASH4.0 V2 sCMOS camera. 100x objective has been used.

5 Construction of the Mathematical Model

In this section, a mathematical model should be constructed on the basis of the former two sections. To do this, the given data must necessarily be simplified, which will subsequently limit the reliability of the model. In order to evaluate to what extent the model will be applicable, I will first present the methods of mathematical modeling and then apply them on the given situation.

5.1 Mathematical modeling and the scientific method

The phenomena in the physical world are influenced and shaped by an immense number of physical parameters and conditions. To make any conclusions about the physical world or alone to describe some specific phenomenon, it is therefore necessary to construct a simplified model first. Only on a basis of such model, one can try to describe the principles behind the observed phenomenon.

Okubo describes this process in [13] as consisting of three steps:

1. Construct an analogy based on observations.
2. Formalize the analogy and formulate it as a model.
3. Make predictions based on the model and introduce a hypothesis or hypotheses that characterize the subject under the consideration.

Subsequently, the hypotheses can be confirmed or rejected by an experiment. The result can be included in a new model and the process repeated several times. The latter approach is often termed scientific method.

5.2 Different Types of Models

Choosing a model with regard to the amount of given information

In cases where the majority of the necessary data is well-known, the steps 1 and 2 from above might appear straightforward without special attention necessary. The "analogies" here are just the ordinary geometric shapes and well established physical laws.

In cases like ours, such straightforward approach is not possible. We have given the cargo final positions on the vacuole, but possess only limited information about the mechanism driving the motion of the autophagosomes. [5] The inadequate informations must be supplemented by some abstract concept substituting the missing part in the model.

Different levels of abstraction

Even if all related information are known, choosing a simplified analogy can help to focus on some aspects of the research, by switching out the less important details. Different types of models differ in their usefulness to make predictions and hypotheses in point (3). By choosing different levels of abstraction in point (1), roughly the following two classes of models can be defined: [6]

- **Simplified models:** By excluding details and using larger degree of abstraction, the model becomes simpler. By extracting the phenomena on which we want to focus and

[5] The above distinction is analogous to the one in [10], where the first case is termed as "white-box" and the second as "black-box" models.

[6] The distinction is taken from [9] and supplemented.

excluding the rest, we get better analytical insight in their functioning and in some cases prevent them from becoming numerically unstable or computationally too large, however the results can become meaningless, when we exclude too many details.

- **Detailed models** where as many as possible components are included into the model in as possible unchanged way. When there are too many unknowns in the studied subject, this can make the model nontransparent and the hypothesis hard to formulate.

5.3 Definition of the Model of the Experiment

5.3.1 The model of the cell

The spatial arrangement used for the model will be very simplified:

Definition 2 *1. The cell will be represented as a ball.*

2. The vacoule will be represented by another ball in the interior of the cell. Other organelles will not be represented.

3. The cell interior without the vacuole will be denoted by $\Omega \subseteq \mathbb{R}^3$

Within Ω, the cargo (i.e. the autophagosome) will be placed:

Definition 3 *The position of the cargo will be represented as a stochastic density* $\rho(x,t)$*, where* $x \in \Omega$ *and* $t \geq 0$*, such that*

$$\rho(x,0) = \rho_{init}(x),$$

for every $x \in \Omega$*, where* ρ_{init} *is a given function representing the probability distribution of the initial cargo location.*

Mostly, ρ_{init} will be concentrated in a small area coinciding with the initial position of the cargo, distributed according to the accuracy of the experimental measurement.

The following assumptions will be formally included latter in the equations 7 and 8:

1. The outer cell membrane is untraversable for the cargo, which will therefore stay in Ω, till it will enter the vacuole.
2. The cargo will enter the vacoule only once; it won't be able to enter partially or leave the vacuole again.
3. Applied on the density $\rho(x,t)$, it will be assumed that the cargo is absorbed with a constant rate $k > 0$ along the surface of the vacuole.

From above assumptions it follows immediately that the cargo will be absorbed to the vacuole exactly once, which will happen in finite time. Therefore one can define:

Definition 4 *The probability distribution of the cargo along the surface of the vacuole after it attaches to it is given by:*

$$\rho_\infty(x) := \int_0^\infty \rho(x,t)dt \tag{1}$$

$$, \forall x \text{ on the surface of the vacuole} \tag{2}$$

5.3.2 The model of motion

The biological and chemical processes presented in the section 3.4 should be converted to a form that can be analyzed by mathematical methods. This will be done in three steps, from the most extensive to the more simplified model. The detailed approach is necessary to keep an overview about which biological details get lost:

1. Detailed Model: One could include all known mechanisms contributing to the motion as components of the model and adjust them with parameters. Among others, this would demand to include the length and position of every filament of the cytoskeleton and to consider under which circumstances the motion along them activates. However, as the types of motion resulting from different mechanisms can be very similar, different combinations of parameter choices wouldn't be recognizable from the measurable results of the experiment. Equivalently; it wouldn't be possible to set up a hypothesis in sense of the point 3 from 5.1, which could verify or reject a type of motion.

2. Model based on the cargo location: Each biological type of motion, if acting alone, produces its own direction of motion. As an approximation, one can abstain from distinguishing between different types directly and fuse the directions of different motion types to a single vector field, where the probability of the direction of motion depends solely on the location of the cargo in the cell interior. This is already a large restriction, which could exclude some patterns of motion. Most notably, the cargo would with some probability move along the filaments immediately after reaching the corresponding location. E.g., here it is not possible to demand the cargo to be present for some time next to the filament prior the motor proteins activate.

   Due to the structure of the cytoskeleton, the vector field would be noncontinuous. The autophagosome would move due to non-directed motion only, till it would encounter some filament and then continue the path along it. By some probability, the object can again detach from the track and again move due to non-directed motion alone. As the non-directed motion (especially diffusion) is less likely, when the object is attached to the filament, the diffusion would mainly assume the role of the conveyor to the filaments.

3. Stochastic model with continuous vector field: In our experiment, the parameters such as the distance between the tracks, their exact curvature or length are unknown and will have to be included stochastically. Instead of describing the directed component of motion explicitly, one can join the probability of the presence of a track, the probability of switching between directed and nondirected motion and the velocity to a single component, which will be termed advection in the following. As it seems reasonable to assume that the filaments are small, numerous and equally likely to be present in each part of the cell interior, the advection can be represented by a smooth and gradual vector field.

   As the nondirected movement is likely to be dominated by diffusion, while the non-diffusion components are likely to bring the same impact, this type will be equated to diffusion in the following sections.

5.3.3 Mathematical definition of motion

Definition 5 *The direction of the advection will be determined by the deterministic vector field, denoted as* $v(t, x)$.
Again t *designates time and* $x \in \Omega$ *the location.*

The diffusion will be defined in a common way by defining a random walk in discrete space, which proceeds in each direction with the same probability; therefrom the first Fick's law derives. Noting that the nondirected motion begins likely by detaching from some filament,

after which the autophagosome moves between different organelles (which could in various ways influence the movement), at this point a different definition could be possible.

To apply the concept of random walk, the x space component of Ω will be represented as one-dimensional discrete space with Δx being the unit interval. Further, the time will be discretized in steps of Δt. It will be assumed that during each time-step Δt, the object moves exactly for one step Δx to the left or to the right. By setting the value of Δx, the intensity of diffusion can be manipulated.

Let $q_x(x,t)$ be the probability that at the time-point t the object will move to the left if it is on the position x. To get diffusion-only model, one should choose $q_x(x,t) = \frac{1}{2}$. To include advection, choose:

$$q_x(x,t) = \frac{1}{2} - \frac{v_x(x,t)\Delta t}{2\Delta x}, \tag{3}$$

where $v_x(x,t)$ is the x-component of $v(x,t)$

Analogously for the other two space directions.

5.4 The Advection-Diffusion Equation

From 3, the advection-diffusion equation can be derived. First set

$$\rho(x, t+\Delta t) = q_x(x+\Delta x, t)\rho(x+\Delta x, t) + (1 - q_x(x-\Delta x, t))\,\rho(x-\Delta x, t), \tag{4}$$

as the object can be on the position x only if it has been either on the position $x-\Delta x$ or $x+\Delta x$ on time-step before.

By inserting 3 to 4 and rewriting it follows

$$\begin{aligned}\frac{\rho(x,t+\Delta t) - \rho(x,t)}{\Delta t} =& \frac{\Delta x^2}{2\Delta t}\frac{\rho(x+\Delta x,t) - 2\rho(x,t) + \rho(x-\Delta x,t)}{\Delta x^2} \\ &- \frac{1}{2}v_x(x,t)\left(\frac{\rho(x+\Delta x,t)-\rho(x,t)}{\Delta x} + \frac{\rho(x,t)-\rho(x-\Delta x,t)}{\Delta x}\right)\end{aligned}$$

By setting $D = \frac{\Delta x^2}{2\Delta t}$ and letting $\Delta x \to 0$ and $\Delta t \to 0$ the advection-diffusion equation derives: [7]:

$$\partial_t \rho(x,t) = D\partial_x^2 \rho(x,t) + v_x(x,t)\partial_x \rho(x,t) \tag{5}$$

Analogously for the other two space directions. After assuming that the diffusion constant equals D in all space directions, it follows

$$\partial_t \rho = D\Delta\rho - \nabla\cdot(\rho v), \tag{6}$$

where Δ and ∇ are taken over all three space dimensions.

Boundary Conditions

Along the cell membrane, which can't be crossed by autophagosome, it will be assumed

$$(-D\nabla\rho + \rho v)\cdot\nu = 0. \tag{7}$$

Here ν is the outward normal vector. Along the vacuole, where the cargo will be absorbed by the rate k, it will be

$$(-D\nabla\rho + \rho v)\cdot\nu = k\rho. \tag{8}$$

[7] The above derivation is mostly taken from [11]

5.4.1 Dimensionless form of the equations

We rescale the equations 6 and 8

- in space direction by setting $x = x_0 \cdot \tilde{x}$, while x_0 is the radius of the vacuole and $\tilde{x}$ is the dimensionless space variable.
- in time with $t = t_0 \cdot \tilde{t}$ and $t_0 = \frac{x_0^2}{D}$

and

- choose velocity vector $\tilde{v}$ such that $v = -\frac{D}{x_0} \cdot \tilde{v}$.

We get

$$\frac{D}{x_0^2}\partial_{\tilde{t}}\rho = \frac{D}{x_0^2}\Delta_{\tilde{x}}\rho + \frac{D}{x_0^2}\nabla_{\tilde{x}} \cdot (\rho\tilde{v}) \tag{9}$$

$$(\frac{D}{x_0}\nabla_{\tilde{x}}\rho + \frac{D}{x_0}\rho\tilde{v}) \cdot \nu = -k\rho \tag{10}$$

After replacing $\tilde{x}$, $\tilde{t}$, $\tilde{v}$ with x, t, v and $\frac{x_0 k}{D}$ with k that becomes

$$\partial_t\rho = \Delta_x\rho + \nabla_x \cdot (\rho v) \tag{11}$$

$$(\nabla_x\rho + \rho v) \cdot \nu = -k\rho \tag{12}$$

In the rescaled equation, there are only the parameters v and k left to change. The following sections deal with analyzing the consequences of different choices for these two parameters with the aim to estimate their size.

5.5 The Choice of Suitable Parameters

The model defined above contains different variable parameters.

To explain the results of the experiment, the parameters must be selected in combinations which are both biologically plausible and simultaneously produce numerically clearly distinguishable results. According to the section 5.1, the experiment will bring meaningful results, if the model with corresponding combination of parameters can be either verified or rejected.

5.5.1 Relation between the Free Parameters and the Measurable Parameters

The manipulable parameters can be roughly classified in two groups:

1. The free parameters resulting from the unknown biological details. In our model these are:
   - The direction of the advection vector v.
   - The proportion between the diffusive and advective component of movement; in the scaled equation 11 this equals $|v|$.
   - The absorption rate k.

   If the above parameter choices are either verified or rejected, then the procedure has been successful and new knowledge has been obtained.

2. The parameters which are directly measurable during the experiment. Most notably:

   - the position of the vacuole
   - the initial position of the cargo

   Changing these two parameters doesn't bring new information directly, but for some of their values, the conclusions from manipulating the unknown biological parameters can become quantitatively better distinguishable. By choosing a cell with corresponding properties, the experiment can deliver qualitatively different information.

5.5.2 The Direction of Advection

In compliance with the section 3.4, the vector $v(x,t)$ will be choosen pointing either

1. to the center of the vacuole (movement along the actin network), or
2. to some other point in the cell (movement along the microtubuli)

Both options can be combined defining a vector field including both in some proportion.

5.5.3 Manipulating $|v|$ and k; Impact on the Cargo Density along the Vacuole

Changing the advective velocity $|v|$ and the absorption rate k has similar and in some cases indistinguishable effects on the final distribution ρ_∞. The densities resulting from different choices should be compared along areas of comparison on the vacuole, predefined in a way to make differences as visible as possible.

Definition 6 *Let T denote the point on the surface of the vacuole which is the closest to the expected value of the initial position of the cargo as given by ρ_{init}.*

Beginning with $|v|$ and a fix $k \gg 0$: It appears plausible to begin with the (in nature impossible) special case $|v| = \infty$. Here the cargo will immediately reach its destination:

1. Assuming the case 1 from 5.5.2, the cargo will instantly land at the closest point on the vacuole; T is therefore the expected value of the landing location.
2. Assuming the case 2, the cargo will instantly reach the point, toward which the vector v is oriented.

From here on:

- Setting k fix and manipulating $|v|$: By diminishing $|v|$, the density ρ_∞ will continuously become more gradually spread. At $|v| = 0$ (the case of diffusion only) will ρ_∞ assume the highest value at the point T; now both in case 1 and 2 from above.
- Setting $|v|$ finite fix and manipulating k:
  - Moderate values of $|v|$:
    For a lower value of k, the cargo will likely move away again after reaching the vacuole. Subsequently, it will be again exposed to the same type of motion. Therefore, setting a lower k could have an impact comparable to setting a higher diffusion (eq. lower $|v|$). However, for higher values of k, this will become less apparent; large k means that the cargo will be absorbed almost always when it reaches the vacuole and increasing it even further won't bring much difference.

– High values of $|v|$ (approximating the case $|v| = \infty$):

If $k \gg 0$ and the cargo on the vacuolar surface moves away from it, it will return very quickly. Therefore, manipulating k won't bring much difference, as long as it stays sufficiently above 0. However, for $k \approx 0$, the cargo can be expected to stay on the surface of the vacuole for a longer time. More explicitly, while the advection force is still pushing the cargo towards the center of the vacuole, it is balanced with the membrane resistance force pushing in the opposite direction. This fixes the cargo inside the thin layer around the vacuole before it is finally absorbed to it. In the section 6 it will be shown that while staying in this thin layer, the cargo can still change its position due to diffusion.

By letting $k \to 0$, the average time till the cargo will be absorbed can be expanded indefinitely. Consequently, the expected duration of the diffusive component motion can be any long. It follows

Lemma 1 *For $|v|$ finite, the density $\rho(x,t)$ along the vacuole will converge towards uniform distribution for $k \to 0$.*

5.5.4 Areas of Comparison

Assuming the case 1 from 5.5.2 of v pointing to the center of the vacuole. As follows from the above, ρ_∞ will now assume the maximal value at the point T for all possible choices of parameters $|v|$ and k. Therefore, T should be chosen as a starting point for defining areas of comparison along the vacuole. From here on two possibilities open; either the cargo density will be distributed symmetric around the point T or nonsymmetric.

Place a straight line l through the cargo initial position and the center of the vacuole and define 12 equidistantly distributed half-circles lying on the cross-sections of the vacuole through this line. As the outer edges of these half-circles run from the point T to the point on the vacuole most distant from T, it will be suitable to compare the cargo density along them.

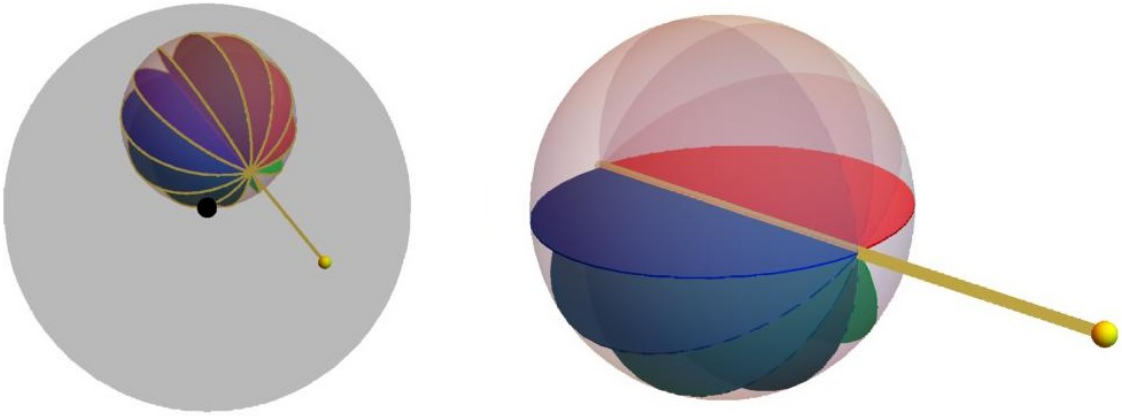

Figure 3: The left side represents a possible layout inside the cell (gray). The yellow dot represents the initial position of the cargo. For the limiting case $|v| = \infty$ the cargo is expected to travel directly to the nearest point on the vacuole along the yellow line. In other cases, the cargo density will be measured along the outer edges (yellow) of the half-circles. The black dot designates the center of the cell. On the right side the layout of the half-circles is represented.

Symmetric Spatial Arrangement

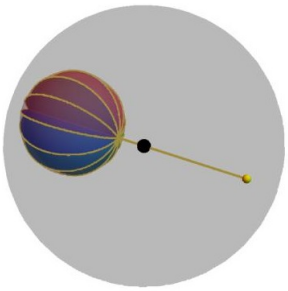

Figure 4: Symmetric spatial arrangement

In the case of symmetric arrangement of the components, i.e. when the center of the cell lyes on l, the distribution resulting from the mathematical model stays the same along each of the half-circles for descending values of $|v|$. Even in diffusion-only case ($|v| = 0$), the highest value of ρ will be taken at T.

This has important implications; during the experiment, if the observed cell is symmetric enough, it can be w.l.o.g. assume that during each repetition of the experiment, the cargo lands on the same halfcircle. So the probability density along one halfcircle can be computed by significantly smaller number of necessary repetitions.

Important: the distribution in the point T and in the point most distant from T affects these two points only. On the contrary, the distribution at the other points along the halfcircle affects larger area as represented in the figure 5:

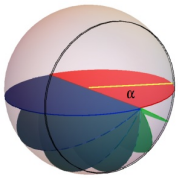

Figure 5: In case of the symmetric layout in the cell, for given α the distribution is equal along the circle (black).

The values of ${}^{e}\rho_{\infty}$ corresponding to $0 \ll \alpha \ll \pi$ in the above figure can be therefore determined with higher degree of accuracy during the experiment.

Non-Symmetric Spatial Arrangement

If l doesn't cross the cell center, the cargo density along a particular half-circle can be influenced by the distance of it from the cell membrane.

For the limiting case $|v| \to \infty$ this is not the case, as the cargo moves only between the initial point and the point T and then slides along the vacuolar membrane if $k \to 0$.

By diminishing the value of $|v|$ and moving away from the above special case, the diffusive motion away from the vacuole becomes important and the shape of the intracellular space starts influencing the final distribution ρ_{∞}.

6 Analytical 2D-Model

In this section, the solution of ρ and ρ_∞ will be analytically approximated for the extreme case of no diffusion and infinite advection velocity.

Assuming $|v| \to \infty$, the cargo will travel towards the vacuole along a straight line through the center of the vacuole and will reach it very quickly. As follows from the section 5.5.3, this can be subdivided in two cases:

1. If $k \gg 0$, the cargo will just attach near the nearest point on the vacuole.
2. If $k \approx 0$, cargo arrives just next to the vacuole, but as it won't be accepted to the vacuole immediately, it stays floating in a thin layer around it.

As the first case is clear, in the following the second will be consider. Therefore it will be assumed:

$$|v| = \frac{1}{\epsilon} \tag{13}$$

$$k = k_1 \epsilon, \tag{14}$$

while $0 < \epsilon \ll 1$.

6.1 The Order of Space and Time; Singular Perturbations

Starting from the initial position, the cargo will reach the vacuole almost instantly, as we assumed $|v| = \frac{1}{\epsilon}$. However, as the absorption coefficient k is of the order $O(\epsilon)$, the necessary time till the cargo will be absorbed to the vacuole, will be of the order $O(\frac{1}{\epsilon^2})$ compared to the first step. Hence, we experience a singular perturbation in the time direction at $t = 0$. To see what happens at this point, the time should be scaled and time units of order $O(1)$ should be replaced with those of time order $O(\epsilon)$.

Similar happens in space directions. Initially ρ_∞ is significantly above zero in comparably large part of the cell. Immediately after $t = 0$ it thickens in the thin layer around the vacuole. At time $t > 0$ it is therefore plausible to scale space and use space units of order $O(\epsilon)$ instead of $O(1)$.

Finally, as the probability density of cargo location thickens around the vacuole, the density itself will reach higher order of value at $t > 0$ as on $t = 0$. It will be therefore rewriten as an asymptotic expansion.

In the rest of the section 6, I will clarify the above and formally show that the movement of the cargo from its initial position till it is absorbed in the vacuole can be divided to three parts:

1. Motion from initial position to the vacuole

   Here I will use the time scale of the order $O(\epsilon)$ and the space scale of the order $O(1)$. (ch. 6.2)

2. Formation of the probability density of cargo location in the thin layer around the vacuole immediately after the cargo reaches the vacuole

   Here both the time and the space scale will be of the order $O(\epsilon)$ (ch. 6.3.1)

3. Cargo motion along the vacuolar membrane due to diffusion

   Here I will again use the time scale of the order $O(1)$, while the space scale will be of the order $O(\epsilon)$ in the direction away from the vacuole and of the order $O(1)$ along the vacuole. (ch. 6.3.2)

6.1.1 Transition to Polar Coordinates

To simplify the expressions, assume that the point $(0,0)$ lies in the center of the vacuole instead in the center of the cell and that the vacuole radius equals 1.

By switching to polar coordinates (r,φ), we can define the thin layer around the vacuole as an area where $r \in (1, 1+\epsilon)$ for some $0 < \epsilon \ll 1$.

Set $\rho(\varphi, r, t) := \rho(x, y, z, t)$ and $\rho_{init}(\varphi, r, t) := \rho_{init}(x, y, z, t)$ for corresponding coordinates as explained in the figure 6.

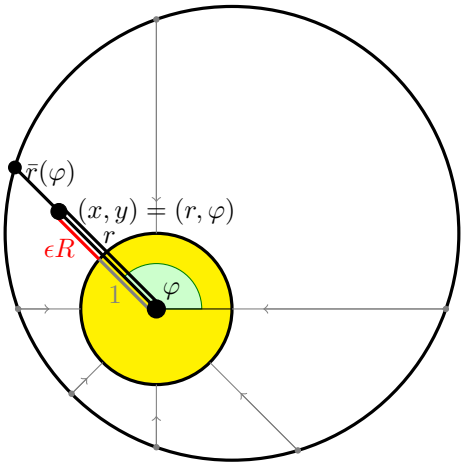

Figure 6: 2D-model:
The white circle represents the cell and the yellow circle represents the vacuole. Assume the point $(0,0)$ is the center of the vacuole and the vacuole has radius 1. Position (x,y) can be described equivalently by polar coordinates (φ, r).
$\bar{r}(\varphi)$ is the distance to the cell membrane for given φ, such that $(\bar{r}(\varphi), \varphi)$ lies on the cell membrane for every φ.
To represent clearly the positions in the thin layer around the vacuole ($r \approx 0$) we split r:
$r = 1 + \epsilon R$

As $r = \sqrt{x^2+y^2}$ and $\varphi = \arctan\left(\frac{y}{x}\right)$, it follows

$$\begin{pmatrix} \partial_x r \\ \partial_y r \end{pmatrix} = \begin{pmatrix} \frac{x}{\sqrt{x^2+y^2}} \\ \frac{y}{\sqrt{x^2+y^2}} \end{pmatrix} = \begin{pmatrix} \cos(\varphi) \\ \sin(\varphi) \end{pmatrix}$$

and

$$\begin{pmatrix} \partial_x \varphi \\ \partial_y \varphi \end{pmatrix} = \begin{pmatrix} \frac{1}{1+\left(\frac{y}{x}\right)^2}\left(-\frac{y}{x^2}\right) \\ \frac{1}{1+\left(\frac{y}{x}\right)^2}\frac{1}{x} \end{pmatrix} = \begin{pmatrix} \frac{-y}{x^2+y^2} \\ \frac{x}{x^2+y^2} \end{pmatrix} = \frac{1}{r}\begin{pmatrix} -\sin(\varphi) \\ \cos(\varphi) \end{pmatrix}$$

Now the equations 7 and 8 can be transformed to polar coordinates:

$$\nabla_{(x,y)}\rho(r,\varphi,t) = \partial_r \rho(r,\varphi,t)\begin{pmatrix} \partial_x r \\ \partial_y r \end{pmatrix} + \partial_\varphi \rho(r,\varphi,t)\begin{pmatrix} \partial_x \varphi \\ \partial_y \varphi \end{pmatrix}$$

$$\begin{aligned} \Delta_{(x,y)}\rho =& \nabla_{(x,y)} \cdot \left(\begin{pmatrix} \cos(\varphi) \\ \sin(\varphi) \end{pmatrix} \partial_r \rho + \begin{pmatrix} -\sin(\varphi) \\ \cos(\varphi) \end{pmatrix} \partial_\varphi \rho \right) \\ =& \left(\begin{pmatrix} \cos(\varphi) \\ \sin(\varphi) \end{pmatrix} \partial_r + \begin{pmatrix} -\sin(\varphi) \\ \cos(\varphi) \end{pmatrix} \partial_\varphi \right) \cdot \left(\begin{pmatrix} \cos(\varphi) \\ \sin(\varphi) \end{pmatrix} \partial_r \rho + \begin{pmatrix} -\sin(\varphi) \\ \cos(\varphi) \end{pmatrix} \partial_\varphi \rho \right) \\ =& \partial_r^2 \rho + \frac{1}{r}\partial_r \rho + \frac{1}{r^2}\partial_\varphi^2 \rho \end{aligned}$$

$$\nabla_{(x,y)} \cdot (\rho v) = \left(\begin{pmatrix} \cos(\varphi) \\ \sin(\varphi) \end{pmatrix} \partial_r \rho + \begin{pmatrix} -\sin(\varphi) \\ \cos(\varphi) \end{pmatrix} \partial_\varphi \rho \right) = -\partial_r \rho - \frac{1}{r}\rho$$

We get

$$\partial_t \rho(r,\varphi,t) = \partial_r^2 \rho(r,\varphi,t) + \frac{1}{r}\partial_r \rho(r,\varphi,t) + \frac{1}{r^2}\partial_\varphi^2 \rho(r,\varphi,t) + \frac{1}{\epsilon}\left(\partial_r \rho(r,\varphi,t) + \frac{1}{r}\rho(r,\varphi,t)\right). \quad (15)$$

6.2 Motion from the Initial Position to the Vacuole

As the motion from item 1 occurs in time $O(\epsilon)$, the equation 15 should be rescaled to described it.

Define a new time unit τ as $\tau = \frac{t}{\epsilon}$. From the eq. 10 it follows:

$$\frac{1}{\epsilon}\partial_\tau \rho(r,\varphi,\tau) = \partial_r^2 \rho(r,\varphi,\tau) + \frac{1}{r}\partial_r \rho(r,\varphi,\tau) + \frac{1}{r^2}\partial_\varphi^2 \rho(r,\varphi,\tau) + \frac{1}{\epsilon}\left(\partial_r \rho(r,\varphi,\tau) + \frac{1}{r}\rho(r,\varphi,\tau)\right) \quad (16)$$

$$\partial_\tau \rho = \epsilon\left(\partial_r^2 \rho + \frac{1}{r}\partial_r \rho + \frac{1}{r^2}\partial_\varphi^2 \rho\right) + \partial_r \rho + \frac{1}{r}\rho \quad (17)$$

Now we let $\epsilon \to 0$ and get the equation:

Lemma 2 *Assume $\tau = \frac{t}{\epsilon}$ where $t = O(1)$ and $r > 1$. Then $\rho \approx \bar{\rho}$ for some $\bar{\rho}$ such that:*

$$\partial_\tau \bar{\rho}(r,\varphi,\tau) - \partial_r \bar{\rho}(r,\varphi,\tau) = \frac{1}{r}\bar{\rho}(r,\varphi,\tau) \quad (18)$$

This equality approximates the movement of cargo prior it reaches the vicinity of the vacuole.

In the thin layer around the vacuole the probability density can grow to infinity and the term under ϵ in the equation 16 doesn't vanish anymore. Therefore the assumption $r > 1$ above.

Note that the equality describes the movement in time and the r-direction only; there is no movement in the direction of φ. For each possible position φ on the vacuole we get a separate equation with corresponding solution.

We introduce two new variables depending on r and τ; $\tilde{r}(r,\tau)$ and $\tilde{\tau}(r,\tau)$.
We want to get

$$\frac{\partial \bar{\rho}(\tilde{r},\tilde{\tau})}{\partial \tilde{\tau}} = \frac{\partial \bar{\rho}}{\partial \tau}\frac{\partial \tau}{\partial \tilde{\tau}} + \frac{\partial \bar{\rho}}{\partial r}\frac{\partial r}{\partial \tilde{\tau}} = \frac{1}{r}\bar{\rho}(r,t) \quad (19)$$

To get the second equality we set $\frac{\partial \tau(\tilde{r},\tilde{\tau})}{\partial \tilde{\tau}} = 1$ and $\frac{\partial r(\tilde{r},\tilde{\tau})}{\partial \tilde{\tau}} = -1$ and insert it to 18.
Possible choices satisfying this conditions are $\tilde{\tau} = \tau$ and $r = \tilde{r} - \tilde{\tau}$, i.e. $\tilde{r} = r + \tau$,
where $\tilde{r} > 1 + \tau \geq 1$ as $r > 1$ and $\tau \geq 0$.
From 19 follows

$$\frac{\partial \bar{\rho}(\tilde{r},\tilde{\tau})}{\partial \tilde{\tau}} = \frac{1}{\tilde{r} - \tilde{\tau}}\bar{\rho}(\tilde{r},\tilde{\tau}), \quad (20)$$

with the initial conditions at $\tau = 0$: $\bar{\rho}(\tilde{r},0) = \rho_{init}(\tilde{r},\varphi)$ and $\bar{\rho}(\tilde{r},\tilde{\tau}) = 0$ for $\tilde{r} = \bar{r}(\varphi) + \tilde{\tau}$

$$\bar{\rho}(\tilde{r},\varphi,\tilde{\tau}) = \bar{\rho}(\tilde{r},\varphi,0)\exp\left(\int_0^{\tilde{r}} \frac{1}{\tilde{r} - \eta}d\eta\right) \quad (21)$$

$$= \bar{\rho}(\tilde{r},\varphi,0)\exp\left(-\ln(\tilde{r} - \tilde{\tau}) + \ln(\tilde{r})\right) \quad (22)$$

$$= \bar{\rho}(\tilde{r},\varphi,0)\frac{\tilde{r}}{\tilde{r} - \tilde{\tau}} \quad (23)$$

$$= \rho_{init}(r + \tau,\varphi)\frac{r + \tau}{r} \quad (24)$$

By assuming that $\rho_{init}(r,\varphi) = 0$ for $r > \hat{r}(\varphi)$, i.e. for the locations outside the cell, it follows:

Lemma 3 *Assume* $\tau = \frac{t}{\epsilon}$ *where* $t = O(1)$ *and* $r > 1$. *Then*

$$\bar{\rho}(r,\varphi,\tau) = \begin{cases} \rho_{init}(r+\tau,\varphi)\frac{r+\tau}{r} & \text{if } r+\tau \leq \hat{r}(\varphi) \\ 0 & \text{if } r+\tau > \hat{r}(\varphi) \end{cases} \tag{25}$$

That means, at the time $\epsilon \cdot \tau$ shortly after the begin the cargo is present in the thin layer around the vacuole with probability almost 1.

6.3 The Motion Close to the Vacuole

To explore what happens in the thin layer around the vacuole ($r \approx 1$), we must scale the equations in the space direction.

We use that $r = 1 + \epsilon R$ and rewrite the equation 15

$$\partial_t \rho(R,\varphi,t) = \frac{1}{\epsilon^2}\left(\partial_R^2\rho + \partial_R\rho\right) + \frac{1}{\epsilon}\left(\frac{1}{1+\epsilon R}\partial_R\rho + \frac{1}{1+\epsilon R}\rho\right) + \frac{1}{(1+\epsilon R)^2}\partial_\varphi^2\rho \tag{26}$$

Analogously we rewrite the border conditions (equation 12):

$$\partial_r\rho(r,\varphi,t) + \frac{1}{\epsilon}\rho = k\rho \tag{27}$$

$$\frac{1}{\epsilon}\partial_R\rho(R,\varphi,t) + \frac{1}{\epsilon}\rho = k\rho = \epsilon k_1\rho \tag{28}$$

$$\partial_R\rho(R,\varphi,t) + \rho = \epsilon k\rho = \epsilon^2 k_1\rho \tag{29}$$

We let and note that the equation 26 consists of parts with different orders of magnitude, i.e. $O(\frac{1}{\epsilon^2})$, $O(\frac{1}{\epsilon})$ and $O(1)$. By letting $\epsilon \to 0$, eq. 27 can be split to 3 separate equations.

As $k = O(\epsilon)$, the motion of cargo along the vacuolar surface ($\partial_\varphi^2\rho$) will take much higher order of time. The equation 26 combines types of motion occuring on different time scales. Therefore, to get the full picture, we have to distinguish between short and long time scale again:

6.3.1 Approximation in Short Time Scale

In the short time scale we approximate how the density thickens around the vacuolar membrane just after the initial time $t = 0$. We set again $t = \epsilon\tau$ and get from the equation 26

$$\frac{1}{\epsilon}\partial_\tau\rho(R,\varphi,\tau) = \frac{1}{\epsilon}\left(\partial_R^2\rho + \partial_R\rho\right) + \left(\frac{1}{1+\epsilon R}\partial_R\rho + \frac{1}{1+\epsilon R}\rho\right) + \epsilon\frac{1}{(1+\epsilon R)^2}\partial_\varphi^2\rho \tag{30}$$

This can be simplified further using $\frac{1}{1+\epsilon R} = 1 + O(\epsilon)$:

$$\partial_\tau\rho(R,\varphi,\tau) = \frac{1}{\epsilon}\left(\partial_R^2\rho + \partial_R\rho\right) + (\partial_R\rho + \rho) + O(\epsilon) \tag{31}$$

Singular perturbation methods and matching

The behavior of $\rho(R,\varphi,\tau)$ at different orders of magnitude will be analyzed by splitting it to two components:

Definition 7 *Define* $\rho_A(R,\varphi,\tau)$ *and* $\rho_B(R,\varphi,\tau)$ *such that* $O(\rho_A) = O(\rho_B)$*, and*

$$\rho(R,\varphi,\tau) = \frac{1}{\epsilon}\rho_A(R,\varphi,\tau) + \rho_B(R,\varphi,\tau) + O(\epsilon), \tag{32}$$

Each of the two components is affected by the dynamics described by equation 31.

The component ρ_A corresponds to the probability density of the cargo location in the thin layer around the vacuole and ρ_B to the density in the rest of the cell. In the following, we will formally show that $\rho_A \to 0$ for $R \to \infty$ (eq. 40).

Moreover, by proving the equation 49, it will follow that on $R = 0$ the contribution of ρ_B to ρ is insignificant compared to ρ_A.

As $\lim_{R\to\infty} \rho_A(R,\varphi,\tau) = 0$ we will get that $\lim_{R\to\infty} \rho(R,\varphi,\tau) = \lim_{R\to\infty} \rho_B(R,\varphi,\tau)$ and consequently

$$\lim_{R\to\infty} \rho_B(R,\varphi,\tau) = \bar{\rho}(0,\varphi,\tau), \tag{33}$$

where $\bar{\rho}$ is as in chapter 6.2.

Application on advection-difusion equation

We take the derivative of the right side of the equation 32 with respect to τ and insert twice the equation 30 with ρ replaced by ρ_A and ρ_B respectively.

$$\frac{1}{\epsilon}\partial_\tau\rho_A + \partial_\tau\rho_B = \frac{1}{\epsilon^2}\left(\partial_R^2\rho_A + \partial_R\rho_A\right) + \frac{1}{\epsilon}\left(\partial_R\rho_A + \rho_A\right) + O(1) \tag{34}$$

$$+ \frac{1}{\epsilon}\left(\partial_R^2\rho_B + \partial_R\rho_B\right) + O(1) \tag{35}$$

To get the border conditions (i.e. on $R = 0$), we insert 32 to 27 and get

$$\frac{1}{\epsilon}\left(\partial_R\rho_A + \rho_A\right) + \left(\partial_R\rho_B + \rho_B\right) = \epsilon k_1\rho \ + O(\epsilon) \text{ on } R = 0 \tag{36}$$

Comparing different orders of magnitude

Scale $O(\frac{1}{\epsilon^2})$ in eq. 34 $\quad \partial_R^2\rho_A + \partial_R\rho_A = 0 \qquad (37)$

Scale $O(\frac{1}{\epsilon})$ in eq. 36 $\quad \partial_R\rho_A(0,\varphi,\tau) + \rho_A(0,\varphi,\tau) = 0 \qquad (38)$

By integrating 37 over R and using 38 as an initial value we get

$$\partial_R\rho_A(R,\varphi,\tau) + \rho_A(R,\varphi,\tau) = 0, \quad \forall R \tag{39}$$

Definition 8 *Define*

$$\rho_0(\varphi,\tau) := \rho_A(0,\varphi,\tau)$$

It follows

$$\rho_A(R,\varphi,\tau) = \rho_0(\varphi,\tau)e^{-R} \tag{40}$$

Similar for the smaller order of magnitude:

Scale $O(\frac{1}{\epsilon})$ in eq. 34

$$\partial_\tau \rho_A = \partial_R^2 \rho_B + \partial_R \rho_B + \underbrace{\partial_R \rho_A + \rho_A}_{=0} \tag{41}$$

$$= \partial_R(\partial_R \rho_B + \rho_B) \tag{42}$$

Scale $O(1)$ in eq. 36

$$\partial_R \rho_B(0,\varphi,\tau) + \rho_B(0,\varphi,\tau) = 0 \tag{43}$$

From 41 we get

$$\int_0^R \partial_\tau \rho_A = (\partial_R \rho_B + \rho_B)\Big|_0^R \tag{44}$$

With 40 follows

$$\int_0^R \partial_\tau \rho_A = \partial_\tau \rho_0 \int_0^R e^{-R} = (1 - e^{-R})\partial_\tau \rho_0 \tag{45}$$

For R large enough we get using 43:

$$\partial_\tau \rho_0(\varphi,\tau) = \partial_R \rho_B(R,\varphi,\tau) + \rho_B(R,\varphi,\tau) \tag{46}$$

As explained in section 6.3.1, from $\rho_A = \rho_0 e^{-R}$ follows that ρ_B matches $\bar{\rho}$ for large R, i.e.

$$\lim_{R\to\infty} \rho_B(R,\varphi,\tau) = \bar{\rho}(1,\varphi,\tau) = \begin{cases} \rho_{init}(1+\tau,\varphi)(1+\tau) & \text{if } 1+\tau \le \hat{r}(\varphi) \\ 0 & \text{if } 1+\tau > \hat{r}(\varphi) \end{cases} \tag{47}$$

It follows that $\partial_R \rho_B(R,\varphi,\tau) = 0$ for R and τ large enough. Inserting this to 46 we get

$$\partial_\tau \rho_0(\varphi,\tau) = \rho_B(R,\varphi,\tau) \tag{48}$$

From the definition 7 it follows that $\rho_0(\varphi,0) = 0$. By integrating over τ we get from the above equation:

$$\rho_0(\varphi,\tau) = \int_0^{\bar{r}(\varphi)-1} \rho_{init}(\varphi,1+\sigma)(1+\sigma)d\sigma \tag{49}$$

$$= \int_1^{\bar{r}(\varphi)} \rho_{init}(\varphi,r)rdr, \quad \forall\tau \text{ large enough.} \tag{50}$$

Alternatively, one could derive the above by considering that $\int_0^\infty \rho_0(\varphi,\tau)e^{-R}dR = \rho_0(\varphi,\tau)$.

6.3.2 Approximation in the Long Time Scale

To describe also the motion in the φ direction, which is of the order $O(1)$ in the equation 26, we will split $\rho(R, \varphi, t)$ to three components with different orders of magnitude:

Definition 9 *Define* $\rho_1(R, \varphi, \tau)$, $\rho_2(R, \varphi, \tau)$ *and* $\rho_3(R, \varphi, \tau)$ *such that* $O(\rho_1) = O(\rho_2) = O(\rho_3)$ *and*

$$\frac{1}{\epsilon}\rho(R, \varphi, t) = \frac{1}{\epsilon}\rho_1(R, \varphi, t) + \rho_2(R, \varphi, t) + \epsilon\rho_3(R, \varphi, t) + O(\epsilon^2) \tag{51}$$

Analogously to the previous chapter, each of the components is affected by the dynamics of the equation 26. Again we take the time derivative of the equation 51, this time using the non-scaled time units:

$$\begin{aligned}\frac{1}{\epsilon}\partial_t\rho_1 + \partial_t\rho_2 + \epsilon\partial_t\rho_3 =& \frac{1}{\epsilon^3}\left(\partial_R^2\rho_1 + \partial_R\rho_1\right) + \frac{1}{\epsilon^2}\left(\partial_R\rho_1 + \rho_1\right) + \frac{1}{\epsilon}\partial_\varphi^2\rho_1 && (52)\\ &+ \frac{1}{\epsilon^2}\left(\partial_R^2\rho_2 + \partial_R\rho_2\right) + \frac{1}{\epsilon}\left(\partial_R\rho_2 + \rho_2\right) + O(1) && (53)\\ &+ \frac{1}{\epsilon}\left(\partial_R^2\rho_3 + \partial_R\rho_3\right) + O(1) && (54)\end{aligned}$$

By inserting 51 to 27 we get

$$\frac{1}{\epsilon}\left(\partial_R\rho_1 + \rho_1\right) + \left(\partial_R\rho_2 + \rho_2\right) + \epsilon\left(\partial_R\rho_1 + \rho_1\right) = \epsilon k_1\rho + O(\epsilon) \quad \text{on } R = 0 \tag{55}$$

Comparing different orders of magnitude:

Scale $O(\frac{1}{\epsilon^3})$ in eq. 52 $\quad \partial_R^2\rho_1 + \partial_R\rho_1 = 0 \qquad (56)$

Scale $O(\frac{1}{\epsilon})$ in eq. 55 $\quad \partial_R\rho_1(0, \varphi, t) + \rho_1(0, \varphi, t) = 0 \qquad (57)$

By integrating 56 over R and using 57 as an initial value we get

$$\partial_R\rho_1(R, \varphi, t) + \rho_1(R, \varphi, t) = 0, \quad \forall R \tag{58}$$

Definition 10 *Define*

$$\hat{\rho}_1(\varphi, t) := \rho_1(0, \varphi, t)$$

We get

$$\rho_1(R, \varphi, t) = \hat{\rho}_1(\varphi, t)e^{-R} \tag{59}$$

In exactly the same way we get the solution for ρ_2:

$$\partial_R\rho_2(R, \varphi, t) + \rho_2(R, \varphi, t) = 0, \quad \forall R \tag{62}$$

In the case of ρ_3, the boundary conditions are no more approximated to zero:
We proceed by integrating the equation 63 using that $\rho_1 = \hat{\rho}_1 e^{-R}$.

Scale $O(\frac{1}{\epsilon^2})$ in eq. 52

$$\partial_R^2\rho_2 + \partial_R\rho_2 + \underbrace{\partial_R\rho_1 + \rho_1}_{=0} = 0 \tag{60}$$

Scale $O(1)$ in eq. 55

$$\partial_R\rho_2(0,\varphi,t) + \rho_2(0,\varphi,t) = 0 \tag{61}$$

Scale $O(\frac{1}{\epsilon})$ in eq. 52

$$\partial_t\rho_1 = \partial_R^2\rho_3 + \partial_R\rho_3 + \underbrace{\partial_R\rho_2 + \rho_2}_{=0} + \partial_\varphi^2\rho_1 \tag{63}$$

$$= \partial_R(\partial_R\rho_3 + \rho_3) + \partial_\varphi^2\rho_1 \tag{64}$$

Scale $O(\epsilon)$ in eq. 55

$$\partial_R\rho_3(0,\varphi,t) + \rho_3(0,\varphi,t) = k_1\rho_1(0,\varphi,t) = k_1\hat{\rho}_1(\varphi,t) \tag{65}$$

$$\int_0^\infty \partial_t\rho_1 dR = (\partial_R\rho_3 + \rho_3)\Big|_0^\infty + (-\partial_\varphi\hat{\rho}_1(\varphi,t)e^{-R})\Big|_0^\infty \tag{66}$$

We insert $\rho_1 = \hat{\rho}_1 e^{-R}$ also on the left side. On the right side we use that $(\partial_R\rho_3 + \rho_3 \to 0$ for $R \to \infty$ and eq. 65. It follows for $t \gg 0$:

$$\left(-\partial_t\hat{\rho}_1(\varphi,t)e^{-R}\right)\Big|_0^\infty = -k_1\hat{\rho}_1 + \partial_\varphi^2\hat{\rho}_1 \tag{67}$$

$$\partial_t\hat{\rho}_1(\varphi,t) = \partial_\varphi^2\hat{\rho}_1 - k_1\hat{\rho}_1 \tag{68}$$

Matching of the short and long time scale

Near $t = 0$ the short and long time scale coincide with each other. By the equation 49 it follows:

$$\hat{\rho}_1(\varphi,\tau) = \hat{\rho}_0(\varphi,\tau\epsilon) = \int_1^{\bar{r}(\varphi)} \rho_{init}(\varphi,r)rdr, \quad \forall\tau \text{ large enough.} \tag{69}$$

6.4 The Density on the Vacuole

The equations 67 and 69 contain all necessary information to compute the density around the vacuole in non-scaled time t:

We expand $\hat{\rho}_1(\varphi,t)$ as Fourier series:

$$\hat{\rho}_1(\varphi,t) = \sum_{k=-\infty}^{\infty} e^{ik\varphi}\psi_k(t) \tag{70}$$

$$\psi_k(t) = \frac{1}{2\pi}\int_0^{2\pi} e^{-ik\varphi}\hat{\rho}_1(\varphi,t)d\varphi \tag{71}$$

From 69 follows

$$\psi_0(0) = \frac{1}{2\pi}\int_0^{2\pi} \hat{\rho}_1(\varphi, 0)d\varphi = \tag{72}$$

$$= \frac{1}{2\pi}\int_0^{2\pi}\int_1^{\overline{r}(\varphi)} \rho_{init}(\varphi, r)rdrd\varphi = \frac{1}{2\pi} \tag{73}$$

To derive $\varphi_k(0)$ for $k \neq 0$, the choice of ρ_{init} must be restricted; it should be constant between the coordinates $\varphi = \delta$ and $\varphi = -\delta$:

Definition 11 *Choose $\delta > 0$. Define*

$$\overset{\delta}{_R}\rho_{init}(\varphi, r) := \mathbb{1}_{|\varphi|<\delta}R,$$

where R is chosen such that $\int_\Omega \overset{\delta}{_R}\rho_{init}(\varphi, r)d\varphi dr = 1$.

For given φ, the value of $\overset{\delta}{_R}\rho_{init}(\varphi, r)$ is equal for all $r \in [1, \overline{r}(\varphi)]$. This was chosen due to the equation 69. Alternatively, one could use any distribution which retains the same value of the integral in 69 and mimic the cargo on the observed initial location in the experiment.

It follows

$$1 = \int_\Omega \overset{\delta}{_R}\rho_{init}(\varphi, r)(x)dx = R\int_{-\delta}^{\delta}\int_1 \overline{r}(\varphi)rdrd\varphi = R\int_{-\delta}\delta\frac{\overline{r}(\varphi)^2 - 1}{2}d\varphi \tag{74}$$

$$R = \left(\int_{-\delta}\delta\frac{\overline{r}(\varphi)^2 - 1}{2}d\varphi\right)^{-1} \approx \left(\delta\left(\overline{r}(0)^2 - 1\right)\right)^{-1}, \tag{75}$$

for δ small enough.

Lemma 4

$$\psi_k(0) \approx \psi_0(0) = \frac{1}{2\pi} \qquad \textit{for } |k\delta| \ll 1$$

Proof:

$$\begin{aligned}
\psi_k(0) &= \frac{R}{2\pi}\int_{-\delta}^{\delta} e^{-ik\varphi}\int_1^{\overline{r}(0)} rdrd\varphi \\
&= \frac{R}{2\pi}\frac{\overline{r}(0)^2 - 1}{2}\frac{e^{-ik\varphi}}{-ik}\Bigg|_{-\delta}^{\delta} \\
&= \frac{R}{2\pi}\frac{\overline{r}(0)^2 - 1}{2}\frac{i(\sin(-k\delta) - \sin(k\delta))}{-ik} \\
&\approx \frac{1}{2\pi}\frac{\sin(k\delta)}{k\delta}
\end{aligned}$$

□

The last step is due to 74. Using the equation 67 it follows

$$\partial_t\psi_k(t) = \frac{1}{2\pi}\int_0^{2\pi} e^{-ik\varphi}\partial_t\hat{\rho}_1(\varphi, t)d\varphi = -k^2\psi_k(t) - k_1\psi_k(t).$$

Now, the Fourier coefficients can be approximated:

$$\psi_0(t) = \frac{1}{2\pi} e^{-k_1 t}$$
$$\psi_k(t) \approx e^{-(k^2+k_1)t} \frac{1}{2\pi} \frac{\sin(k\delta)}{k\delta} \approx \psi_{-k}(t)$$

From $\psi_k e^{ik\varphi} + \psi_{-k} e^{-ik\varphi} \approx 2\psi_k \cos(k\varphi)$ follows

$$\hat{\rho_1} \approx \psi_0(t) + \sum_{k=1}^{\infty} 2\psi_k(t) \cos(k\varphi) \tag{76}$$
$$\approx \frac{1}{2\pi} e^{-k_1 t} + \frac{1}{\pi} \sum_{k=1}^{\infty} e^{-(k^2+k_1)t} \cos(k\varphi). \tag{77}$$

Now, the final cargo distribution along the vacuole can be derived:

Theorem 1 *If* $\rho_{init} = {}^{\delta}_{R}\rho_{init}(\varphi, r)$*, then for* $\delta \to 0$ *it follows:*

$$\rho_\infty(\varphi) \approx \frac{1}{2\pi k_1} + \frac{1}{\pi} \sum_{k=1}^{\infty} \frac{1}{k^2 + k_1} \cos(k\varphi) \tag{78}$$

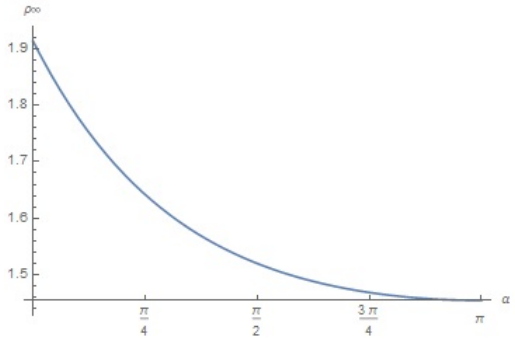

Figure 7: Numerical evaluation of 78 for the choice $k_1 = 1$ and the sum taken from 1 to 1000.

7 Numerical Simulation

The numerical computations has been done by Wolfram Mathematica 11.2.0.0[8]. In this section, the computations will be described in summarized and shortened way. The Mathematica-code is presented in the appendix.

7.1 Assumptions

If not stated otherwise, the numerical computations will be done by assuming the following:

1. The cell is centered in $(0, 0, 0)$ and has radius `cellR` $= 1$
2. The vacuole centered in `vacC` $= (-0.4, 0, 0)$ has radius `vacR` $= 0.4$.
3. The initial distribution of the cargo location is defined using the multivariate normal distribution with the mean value in `initC` $= (0.7, 0, 0)$ and the covariant matrix $\begin{pmatrix} 0.02 & 0 & 0 \\ 0 & 0.02 & 0 \\ 0 & 0 & 0.02 \end{pmatrix}$

   More explicitly, ρ_{init} is given by

   ```
   ρinit[x_, y_, z_]:=
   (1/c)*PDF[MultinormalDistribution[initC,{{0.02,0,0},{0,0.02,0},{0,0,0.02}}],{x,y,z}];,
   ```

   Where c is chosen such that $\int_\Omega \rho\texttt{init} dx = 1$.

7.2 Finite Elements Method

The solutions of the equations 11 and 12 will be approximated with the predefined function `NDSolve`. The function computes an approximation using mainly the finite elements method, which is combined with many other approximation methods. In this section, the finite element method will be presented to an extent necessary to justify the choice of a mesh, by which the region Ω will be partitioned, while the majority of other details will be omitted.

The finite element method consists of the following steps:

1. By defining a mesh, the definition area Ω should be partitioned to smaller compartments which are called finite elements. In our case they will have form of tetrahedrons. The diameter of each of the tetrahedrons will play a crucial role for the size of the error. Furthermore, the shape of the compartments must be taken into account:

   - large angles (near 180°) can cause large interpolation errors
   - small angles (near 0°) can cause the matrix of the linearized problem to be ill conditioned
   - small or skinny elements can induce instabilities in explicit time integration methods

   Depending on the shape of the definition area, it is not always possible to avoid all of the above. In our case, the geometry of the intracellular space allows us to choose tetrahedrons with approximately same-sized angles, however an exception is the case of the vacuole adhering to the cell-membrane.

2. In these smaller compartments, the equation will be multiplied by the test-function $\Phi(x, t)$ and the function will be approximated using methods from the calculus of functional variations. Most notably, a finite dimensional subspace of the particular functional space should be chosen and the variational equation solved over it.

[8] Some explanations of this section are partly taken from the Wolfram Language & System Documentation Center.

7.3 Segmentation of Ω with a Suitable Mesh - Desired Degree of Accuracy

The function `NDSolve` uses a combination of different functional variations selected automatically to minimize the error in the concerned finite element. The error can be further minimized either by setting the number of digits of precision maintained during the computation or, in accordance with the previous chapter, by adapting the partition of Ω.

We will assume 1 % deviation from ρ_∞ to be the largest acceptable and seek to minimize it further when possible. As there are many biological factors not included in the model, it is unlikely that the errors of this size would make the model less applicable on the experiment.

A mesh can be generated using the build-in function `ToElementMesh`. The most obvious choice is to divide Ω to cells of approximately equal size. By lowering the parameter `MaxCellSize`, which sets an upper bound for the cell size, the desired accuracy can be achieved. Simultaneously, the computation complexity rises. This causes the program first to slow down and then to stop working for even smaller values.

This issue can be solved by using denser mesh in the areas, where the functional variations used by `NDSolve` give less accurate results and by using less dense mesh in the other areas.

In our model of the cell interior, different behavior could be expected in the following areas:

- the surface of the vacuole
- the cell membrane
- the area around the initial point
- the rest of the cytoplasm

To get a mesh with the desired properties, Ω will be partitioned to compartments, which should be fitted with a mesh of lower or higher density using the function `ToElementMesh`. An applicable mesh must consist of elements exactly fitting each other on each complementary face. To achieve this, first a 2D-mesh will be defined along the boundaries of the compartments using the function `ToBoundaryMesh`. To match the shape of a tetrahedron mesh in the interior, the boundary mesh will consist of triangles. Subsequently, smaller or larger tetrahedrons will be generated on each side of the border between compartments matching the triangles.

After trying many different meshes, it reveals that a denser mesh on the surface of the vacuole is necessary to keep the error small. The other three choices show far less improvement, including the area around the initial point, where ρ is very high at $t = 0$ and changes very quickly. This indicates that the boundary conditions along the vacuole are the main factor disproportionately affecting the accuracy.

7.3.1 Definition of the Mesh

Define a sphere `wrap` surrounding the vacuole, with the center in `vacC` and the diameter `vacR+0.3`, which will limit the area with a denser mesh. On this sphere, on the cell membrane and on the vacuole apply the function `ToBoundaryMesh` and join all three to a single element as presented on the left side in the figure 8. When `wrap` intersects with the cell membrane or when it gets to close to it, then the mesh elements would interrupt each other. Therefore when a part of the sphere is less than 0.01 away from the membrane, the affected part will be replaced with a corresponding part of the sphere slightly smaller than the cell, with the center in $(0, 0, 0)$ and the radius `cellR-0.01`, to become a continuous surface as depictured in the figure 8. Thereafter, `ToElementMesh` will be applied to define the mesh inside of both compartments. Around the vacuole the `MaxCellSize` will be set to 0.05 and elsewhere to `Automatic`.

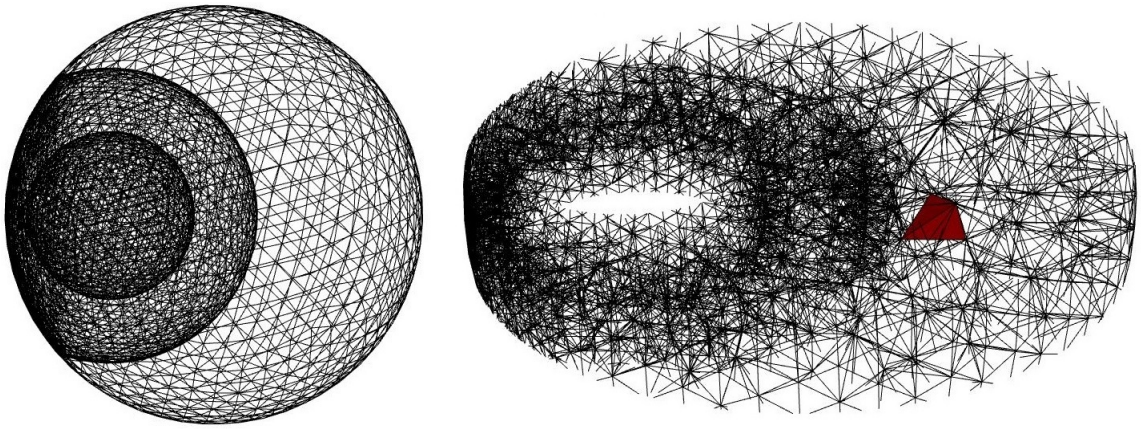

Figure 8: The graphics on the left side represents the 2D-mesh along the boundaries of the compartments defined above. On the right side a cross-section through the cell is represented together with the edges of the tetrahedral finite elements. As an example, one of the tetrahedrons is shown in whole (red).

Mesh adapted for large values of $|v|$

For increasing values of $|v|$, the mesh presented above must be more and more refined in order to get satisfactory results. If $|v|$ exceeds 50, this becomes impracticable to do with an ordinary personal computer. However, as for this values the cargo is expected to travel almost straightforwardly towards the vacuole, large parts of Ω can be excluded from the computation.

Therefore, the mesh will be constructed on a subset $\Omega 1 \subseteq \Omega$. In the later sections, two choices for $\Omega 1$ will be used:

Let l be the line from `vacC` to `initC` and u be the unit vector on it. Define a right cone `cone1` with l as a centerline and the base which intersects the vacuole where $\alpha = \frac{\pi}{2}$. The tip of the cone should be at `initC`$+0.1 \cdot u$.

To represent the section of the vacuole inside `cone1`, define `regA` to contain parts of the ball with center in the point `vacC` and radius `vacR`, which are less than 0.01 away from the border of `cone1`.

Set $\Omega 1 =$ `cone1` $\setminus$ `regA`

For $|v|$ and k large enough, the shape $\Omega 1$ corresponds to the shape of Ω everywhere where ρ is expected to be noteworthy above zero. Again, the boundaries of `regA` and `cone1` will be partitioned to 2D-meshes of different densities.

As both areas nowhere stick to each other, 2D-meshes can be constructed by the function `ToBoundaryMesh`.

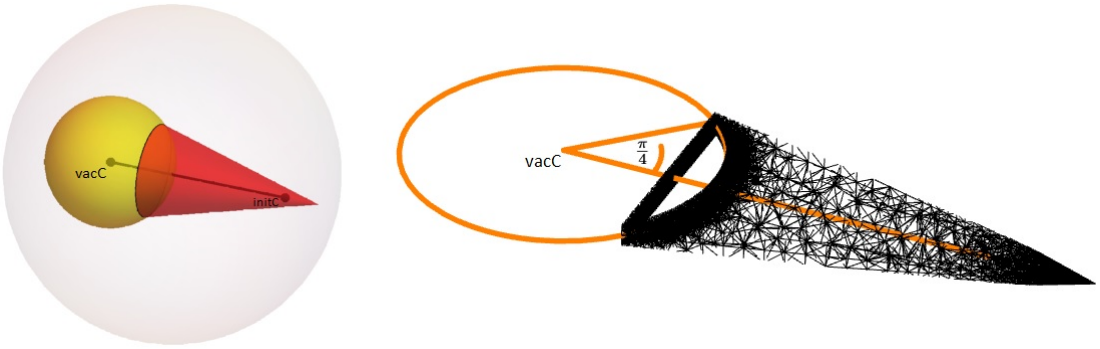

Figure 9: On the left: The value of ρ will be approximated only in the area $\Omega 1$ represented in red. On the right: Cross-section through the mesh: the elements are smaller along the surface of the vacuole (orange circle).

Analogously to 12, the boundary conditions will be set as

$$(\nabla_x \rho + \rho v) \cdot \nu = \begin{cases} -k\rho, \text{ along } \texttt{regA} \\ 0, \text{ along } \texttt{cone1} \end{cases} \tag{79}$$

7.4 Implementation of the Boundary Conditions

An important part of the internal computations of `NDSolve` is done using the weak form of the differential equation. The affected equation will be multiplied by the test function $\Phi(x,t)$ and integrated over the domain. In our case we get from the equation 11:

$$\int_\Omega \nabla \left(-\nabla\rho - v\rho\right) \Phi + \partial_t \rho \Phi \; dx\, dy\, dz = 0 \tag{80}$$

Integration by parts delivers

$$\int_\Omega \left(\nabla\rho + v\rho\right) \nabla\Phi + \partial_t \rho \Phi \; dx\, dy\, dz = \int_{\partial\Omega} \left(\nabla\rho + v\rho\right) \Phi \cdot \nu \; dx\, dy\, dz \tag{81}$$

The ν is again the outward normal vector. The expression $(\nabla\rho + v\rho) \cdot \nu$ on the right hand side will be replaced by the corresponding value of the flow through the boundary as it follows from the equation 12. This will be implemented to `NDSolve` with the option `NeumannValue`.

$$\int_{\partial\Omega} \left(\nabla\rho + v\rho\right) \Phi \cdot \nu \; dx\, dy\, dz = \begin{cases} \int_{\partial\Omega} -k\rho\Phi \; dx\, dy\, dz & \text{on the vacuolar membrane} \\ 0 & \text{on the cell membrane} \end{cases} \tag{82}$$

$$= \begin{cases} \texttt{NeumannValue}[-k\rho] & \text{on the vacuolar membrane} \\ \texttt{NeumannValue}[0] & \text{on the cell membrane} \end{cases} \tag{83}$$

7.5 Evaluating the Distribution ρ

7.5.1 ρ_∞ in Finite Time

To approximate ρ_∞, the function ρ will be integrated over time from 0 to `tStop`. Here `tStop` can be chosen as any time, where the cargo location density in the whole cell interior is small enough, but it shouldn't be to large to avoid numerical instabilities. To implement this choose `tStop` such that $\int_\Omega \rho(x, \texttt{tStop}) d\Omega < 0.001$.

Define

$$\rho\texttt{Fin} := \int_0^{\texttt{tStop}} \rho(x,t)\ dt,$$

where x is a position on the surface of the vacuole.

7.5.2 Points of Comparison

Now the indicators defined in the section 5.5 can be computed. The distribution $\rho\texttt{Fin}$ will be computed along the half-circles on the cross-section through the vacuole as defined in the section 5.5.4.

The function `NDSolve` will output $\rho(x,t)$ in a form of an `Interpolating Function` object, which means that ρ will be represented by a set of numerical values and interpolation rules between them. The numerical outcome of $\rho(x,t)$ for given x and t is yet to be computed. This makes numerical integration of an `Interpolating Function` object very time-consuming. This problem can be avoided by restricting the integration to only 11 points of comparison distributed equidistantly along each of the slices. Due to geometrical arrangement, the first and the last point are shared between all of the slices. For the cases of very steep distribution of $\rho\texttt{Fin}$ (where $|v|$ is very high compared to k), an alternative layout of points will be used (here with 29 points).

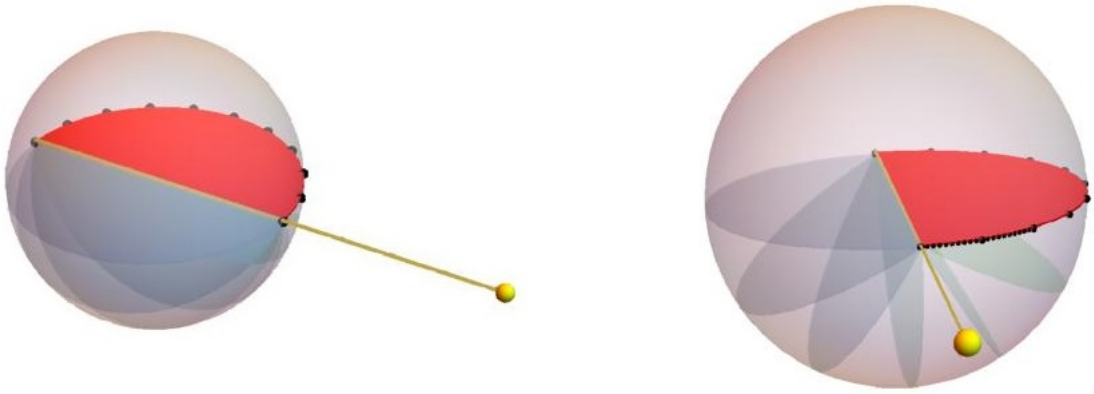

Figure 10: Positions of the points of comparison along one of the slices. Along the other slices they are positioned analogously.
On the right: Here additional 9 points are added between 1^{st} and the 2^{nd} point and 9 between 2^{nd} and the 3^{rd}.

7.6 The Numerical Results

7.6.1 Symmetric Spatial Arrangement

In the case of symmetric spatial arrangement, as defined in section 5.5.4, the cargo density resulting from the model is expected to be the same along all of the half-circles. To analyze this case, it therefore suffices to approximate $\rho\texttt{Fin}$ along only one of the half-circles. In the following, I used the one lying on the y-positive half of the x-y-plane. In the section 8.4, to the nonsymmetric case will be considered, where $\rho\texttt{Fin}$ will be evaluated separately along each of the 12 half-circles.

7.6.2 The case without advection

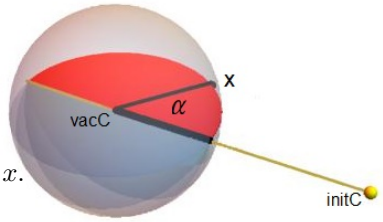

Assume x is a point on the surface of the chosen half-circle. To designate the location of x, define α to be the angle in the point `vacC` defined between the line through `vacC` and `initC` and the line through `vacC` and x.

Assume $|v| = 0$ and $k = 1$. Represent α on x-axis and ρ`Fin` on y-axis:

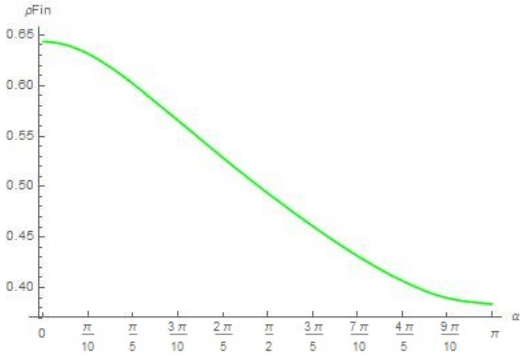

The graph confirms, that even in the case of diffusion only, for moderate value of k the differences in the density are large enough to be measurable in the experiment.

7.6.3 The Range of the Parameters

As defined in the section 5.4.1, the parameters $|v|$ and k are dimensionless. From definition follows that $|v| \geq 0$ and $k > 0$, but there are no direct biological informations which would make possible to limit their range. Therefore, to estimate which range of the parameter choices is biologically relevant, all combinations should be considered, which can be distinguished by the distribution of ρ`Fin`.

Limiting the parameters from above

Assume that there is no diffusion, equivalently $|v| \to \infty$. Assume $k \gg 0$. Therefore, the cargo will be absorbed to the vacuole on the closest position on it.

If the initial position of the cargo were given as a single point, then the cargo would be absorbed to the vacuole at the position $\alpha = 0$. On the contrary, with the initial position of the cargo given by the distribution `initC`, it follows analogously to the equation 25 :

$$\overline{\rho_\infty}(\alpha) = \int_0^{\overline{r}(\varphi)} \frac{(\texttt{vacR} + s)^2}{\texttt{vacR}^2} \texttt{initC}\left(x + s \cdot (-\vec{\nu})\right) ds. \tag{84}$$

Evaluating 84 numerically returns:

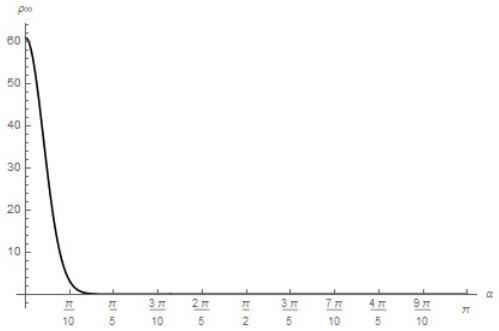

Figure 11: Distribution along the vacuole with given initial distribution `initC`, assuming the cargo is absorbed at the nearest point on the vacuole.

For $k \gg 0$, the distribution ρ`Fin` is therefore expected to approximate $\overline{\rho_\infty}$ for large values of $|v|$. Increasing $|v|$ even further wouldn't change the measurable results, therefore this will be avoided.

The results in section 6 however indicate that there is no $|v| > 0$ such that ρ`Fin` would approximate $\overline{\rho_\infty}$ for arbitrarily small values of $k > 0$.

For $k = 1$ or higher, ρ`Fin` will approximate $\overline{\rho_\infty}$ at around $|v| = 200$.

Limiting the parameter k from below

As explained in the section 5.5.3, by decreasing the value of k, the cargo probability density will become more equally distributed and for k small enough, the ρ_∞ will approximate the uniform distribution. To find a numerical example for this, note that the largest value of ρ`Fin` along the half-circle is expected at the position $\alpha = 0$ and the smallest at $\alpha = \pi$. For the choice $|v| = 0$ and $k = 0.01$ it is

$$|\rho\texttt{Fin}(0) - \rho\texttt{Fin}(\pi)| < 0.01.$$

Manipulating the parameter |v|

The case of ρ`Fin` being almost uniform distribution appears to be a suitable starting point to compare the effects of increasing $|v|$ and k. Fix $k = 0.01$ and increase $|v|$ in steps of 5.:

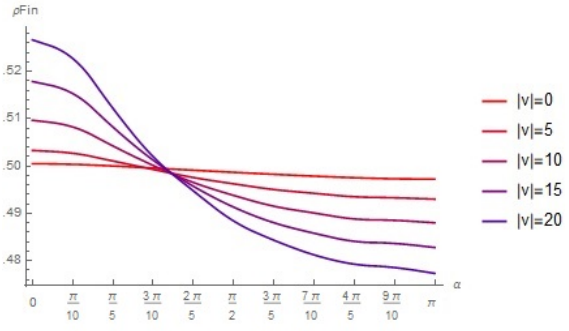

Figure 12: k=0.01 fix

Manipulating the parameter k

Fix $|v| = 0$ and compare different values of k:

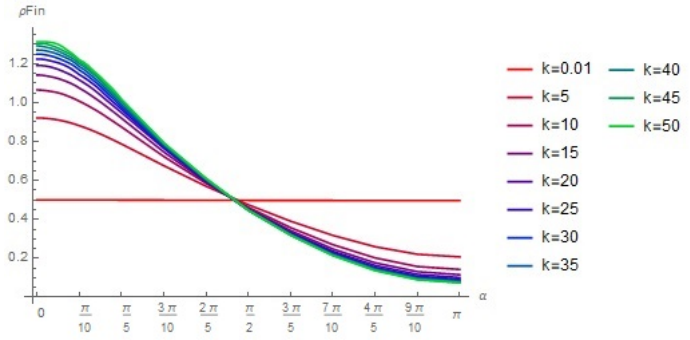

Figure 13: The distribution $\rho\texttt{Fin}$ along the half-circle for different values of k with $|v| = 0$ fix.

Analogously as before, $\rho\texttt{Fin}(0)$ should be compared for different values of k:

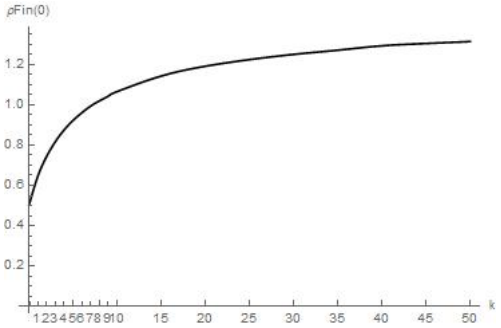

Figure 14: The value of $\rho\texttt{Fin}(0)$ depending on k for fix $|v| = 0$

The curve in the figure 14 slows down significantly for larger k. This confirms the prediction in the section 5.5.3: a very large k means that the cargo will be almost immediately absorbed if it reaches the vacuole. Consequentially it will be almost surely absorbed on the place of the first contact with the vacuole, while the position of the first contact is not influenced by the value of k. However, for high values of k, the approximation becomes increasingly numerically unstable, therefore it is not possible to numerically approximate the value to which $\rho\texttt{Fin}(0)$ converges for $k \to \infty$.

8 Invertability of the Results

8.1 Distinguishable and Indistinguishable Combinations of Parameters

The results in the above section and the considerations in the section 5.5.3 suggest that it is not always possible to distinguish between different choices of $|v|$ and k. By increasing $|v|$, the value of $\rho_\infty(0)$ will rise, but it can be lowered to the same value as before by decreasing k.

Lemma 5 *For given value $\rho_\infty(0)$, the possible choices of parameter $|v|$ can be represented by a strictly decreasing function $|v|(k)$ defined on the interval $(0, \infty)$.*

The combination of both parameters can be determined only when the value of ρ_∞ along the rest of the half-circle provides enough additional information. This is not always the case. For instance, the choice of $|v| = 5$ and $k = 10$ provides almost (but not exactly) the same distribution along the half-circle as the choice of $|v| = 8.72$ and $k = 3$.

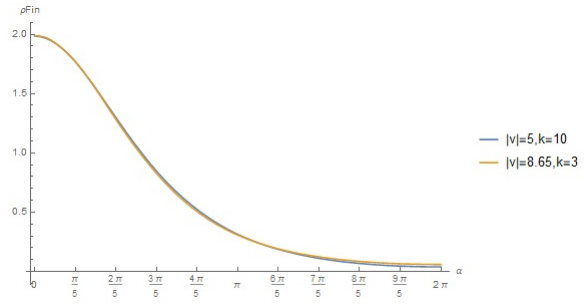

On the contrary, by choosing $|v| = 8.75$, $k = 0.5$ and $|v| = 0.27$, $k = 6$ respectively, the value coincides in the point $\alpha = 0$, but differs substantially at $\alpha = \pi$.

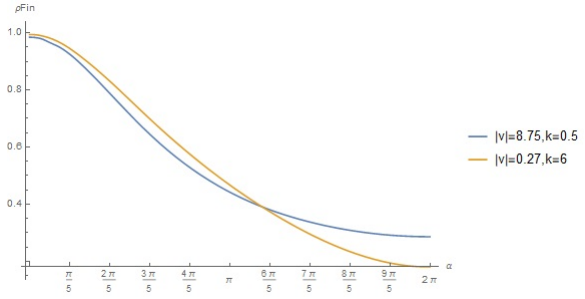

The above example belongs already to the better distinguishable cases - there is a comparably large interval (about $\frac{\pi}{10}$ long) where the $\rho\texttt{Fin}(\pi)$ is almost 0 in the first case (orange) and clearly above 0 in the second case. As it will be explained later, this is rarely the case for moderate values of $|v|$. On the contrary, when comparing two cases with the same value of $\rho\texttt{Fin}(0)$, the interval useful for comparison becomes short for large values of $\rho\texttt{Fin}(0)$, which can be concluded by a simple geometric consideration (Note that $\int_\Omega \rho\texttt{Fin}(0)d\Omega$).

8.2 Computation of $|v|$ and k

8.2.1 The value of $\rho\texttt{Fin}(0)$

To expand the above considerations on the whole range of parameters, compare first the values of $\rho\texttt{Fin}(0)$ for different choices of k and $|v|$:

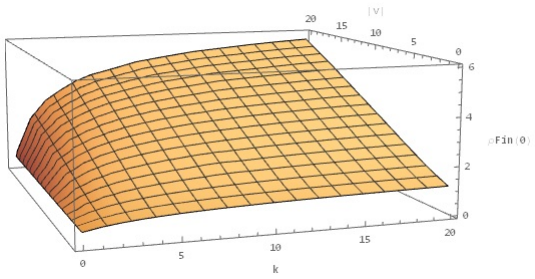

Figure 15: The value of $\rho\texttt{Fin}(0)$ for $k \in (0, 20]$ and $|v| \in [0, 20]$

Analogous to lemma 5, a function $|v|(k)$ can be defined for each given value of $\rho\texttt{Fin}(0)$:

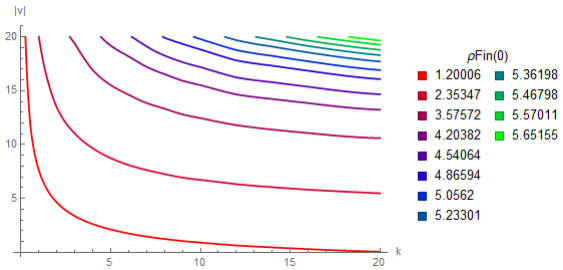

Figure 16: Contour lines retaining the same value of $\rho\texttt{Fin}(0)$, starting at $|v| = 20$ and k gradually distributed between 0 and 20.

If $\rho\texttt{Fin}(0)$ is low, then the possible range of k is limited. This brings qualitatively different behavior:

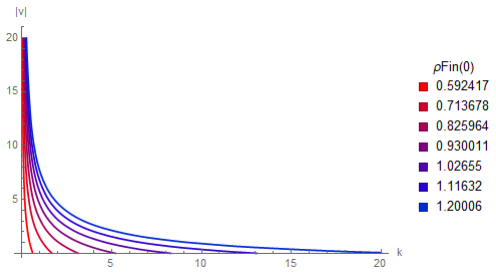

Figure 17: The same as above, with k chosen between 0.03 and 0.15

8.2.2 Applicability of the Values of $\rho\texttt{Fin}(\alpha)$ for $\alpha > 0$

The aim of this section is to explain when evaluating an additional position $\overline{\alpha} \in [0, \pi]$ can help to determine $|v|$ and k and which choice for α_t is most appropriate.

The examples in the section 8.1 show that some choices of $|v|$ and k are indistinguishable even by comparing $\rho\texttt{Fin}(\alpha)$ for all possible $\alpha \in [0, \pi]$, while some combinations of $|v|$ and k can be excluded by analyzing $\rho\texttt{Fin}(\alpha)$ for more than one value of α. In the following the ranges of parameters should be found, where the $|v|$ and k can be uniquely determined.

Noting that the integral of ρ_∞ over the whole cell must equal 1, it follows:

Lemma 6 *Assume the symmetric layout of the cell components. Let ρ_∞ be given for two different combinations of $|v|$ and k; denote it ${}^1\rho_\infty$ and ${}^2\rho_\infty$. Then there must be some $\alpha_s \in (0, \pi)$ such that ${}^1\rho_\infty(\alpha_s) = {}^2\rho_\infty(\alpha_s)$.*

Switching back to the numerical approximation $\rho\texttt{Fin}(\alpha)$, the results presented in the figure 13 shows that $\alpha_s \approx \frac{\pi}{2}$ for $|v| = 0$.

From geometric layout of the cell model it is easy to conclude that the function $\rho_\infty(\alpha)$ is strictly falling. The second derivative $\rho''_\infty(\alpha)$ could change the sign twice, once because the effects of diffusion are becoming more important for rising α and once due to harder accessibility of the region beyond $\alpha = \frac{\pi}{2}$. The numerical approximations show that the latter is not the case.

Lemma 7 *The function $\rho''\texttt{Fin}(\alpha)$ is:*

1. *negative near $\alpha = 0$*
2. *it changes the sign exactly once*

From this follows:

Lemma 8 *Assume ${}^1\rho_\infty(\alpha) \neq {}^2\rho_\infty(\alpha)$. Then $|{}^1\rho_\infty(\alpha) - {}^2\rho_\infty(\alpha)|$ has exactly 2 maximums in $[0, \pi]$.*

To get the most clear result, one should seek to maximaze $|{}^e\rho\texttt{Fin}(\overline{\alpha}) - {}^h\rho\texttt{Fin}(\overline{\alpha})|$, where ${}^e\rho\texttt{Fin}(\overline{\alpha})$ is the result acquired through the experiment and ${}^h\rho\texttt{Fin}(\overline{\alpha})$ any hypothetical $\rho\texttt{Fin}$ with ${}^e\rho\texttt{Fin}(0) = {}^h\rho\texttt{Fin}(0)$.

To achieve this, $\overline{\alpha}$ should be chosen

1. Far enough from $\alpha = 0$.
2. Far enough from $\alpha = \alpha_s$. The latter however differs for different ${}^h\rho\texttt{Fin}$.
3. If ${}^e\rho\texttt{Fin}(\beta) = 0$, then $\overline{\alpha}$ should be chosen should be chosen far enough from $[\beta, \pi]$, as ${}^h\rho\texttt{Fin}(\beta)$ would at this point stay the same for a broad range of $|v|$ and k. If ${}^e\rho\texttt{Fin}(\beta) \approx 0$, then $[\beta, \pi]$ should also be avoided; otherwise a much higher degree of accuracy during the experiment and computation would be needed.

8.2.3 The Value of $\rho\texttt{Fin}(\pi)$

As it follows from above, $\rho\texttt{Fin}(\pi)$ is applicable only when it is clearly larger then 0. At $\alpha = \pi$ this is not the case for most inspected values of $|v|$ and k.

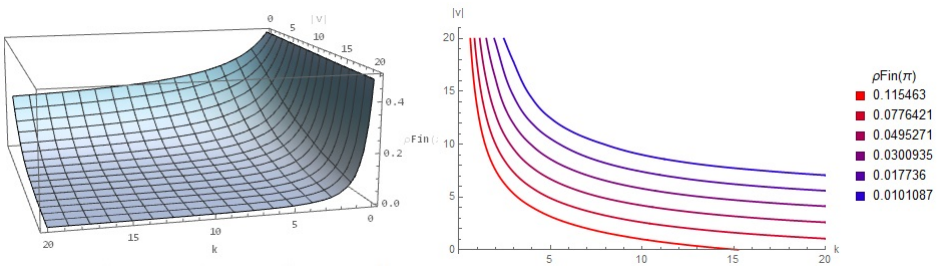

Figure 18: On the right: Note that larger values of $|v|$ and k are very sensitive for small changes of $\rho\texttt{Fin}(\pi)$

For the choices where $\rho\texttt{Fin}(\pi)$ is small enough, the corresponding contour lines of $|v|(k)$ can be compared with those corresponding to $\rho\texttt{Fin}(0)$:

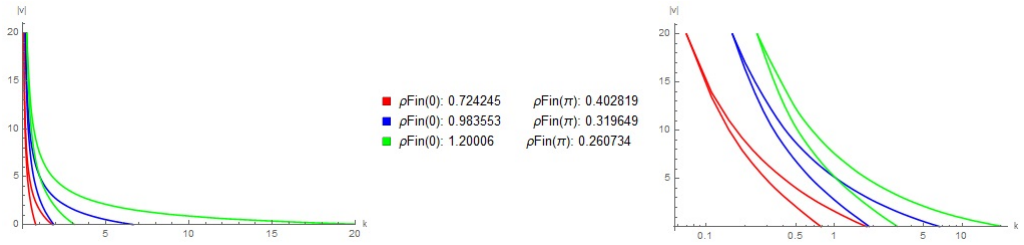

Figure 19: The contour lines run through the points $(k, |v|)$ with $|v| = 20$ and $k = 0.07$, 0.16 and 0.25. They come in pairs; in each pair the upper contour line represents constant value of $\rho\texttt{Fin}(0)$ and the lower the constant value of $\rho\texttt{Fin}(\pi)$. On the right side: the same graph in logarithmic scale. The graph shows only an example of possible values; however by choosing $\rho\texttt{Fin}(\pi)$ anywhere in $[0.05, 0.5]$ a similar pattern occurs.

The distinct inclinations corresponding to $\rho\texttt{Fin}(0)$ and $\rho\texttt{Fin}(\pi)$ show that there must be an unique numerical solution for $|v|$ and k if ${}^{e}\rho_{\infty}(\pi)$ resulting from the experiment lies approximately in $[0.05, 0.5]$.

8.2.4 The Value of $\rho\texttt{Fin}(\frac{7\pi}{10})$

Some of the cases where ${}^{e}\rho_{\infty}(\pi)$ is too small can be dealt with by choosing a smaller α_t, here $\alpha_t = \frac{7\pi}{10}$:

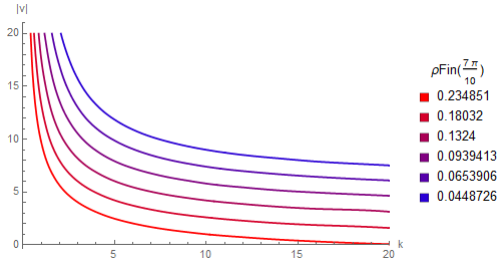

Figure 20: $\rho\texttt{Fin}(\frac{7\pi}{10})$: The contour lines are chosen to run through the points $(k, |v|)$ with $k = 10$ and $|v| = 1, 3, 5, 7, 9$ respectively.

The above results should be compared with analogous results for $\rho\texttt{Fin}(0)$:

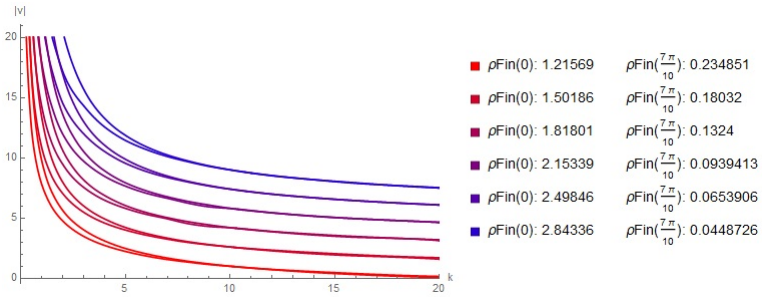

Figure 21: The contour lines run through the points $(k, |v|)$ with $k = 10$ and $|v| = 1, 3, 5, 7, 9$ as above. They come in pairs; in each pair the upper contour line represents $\rho\texttt{Fin}(0)$ and the lower $\rho\texttt{Fin}(\frac{7\pi}{10})$.

Contrarily to the figure 19, the contour lines coincide for k large enough. For smaller k this is not the case.

8.2.5 Distributions with $\rho\texttt{Fin}(\pi) \approx 0$

The case where the given $\rho\texttt{Fin}$ is close to 0 at $\alpha = \pi$ corresponds to large $|v|$ or k. Consequently, the diffusion has much lesser impact on the distribution $\rho\texttt{Fin}$; one can expect that the latter will become more similar to the figure 11. The diffusion becomes limited to small-scale movements, which makes it's impact on $\rho\texttt{Fin}$ comparable to the choice of a lower k. This suggests that $\rho\texttt{Fin}$ could be uniquely determined by given $\rho\texttt{Fin}(0)$, as choosing different combinations of k and $|v|$ now affects the whole half-circle in similar way. Indeed, for $|v|$ and k large enough, $\rho\texttt{Fin}$ differ only in small scale at $\alpha \neq 0$ if they coincide for $\alpha = 0$.

In the case of $|v| = 9$ and $k = 10$ in the figure 21 (the most upper pair), the contour lines relating to $\rho\texttt{Fin}(0)$ and $\rho\texttt{Fin}(\frac{7\pi}{10})$ cross $|v| = 20$ at $k = 2.07$ and $k = 1.5$; the comparably large difference however only reflects that $\rho\texttt{Fin}(\frac{7\pi}{10}) \approx 0$.

At $\alpha = \frac{2\pi}{5}$ the choice $|v| = 9$ and $k = 10$ corresponds to $|v| = 20$ and $k = 2.01$. However, the difference between ${}^{1.5}\rho\texttt{Fin}$ and ${}^{2.01}\rho\texttt{Fin}$ stays small again, as can be anticipated from the distribution of $\rho\texttt{Fin}(\frac{7\pi}{10})$ depending on $|v|$ and k:

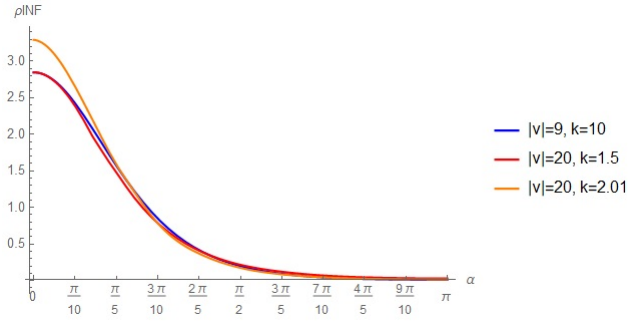

Figure 22: The blue curve representing the case of $|v|$=9 and k=10 compared with distributions coinciding on $\alpha = 0$ and $\alpha = \frac{\pi}{5}$ respectively. The blue and orange curves are almost identical.

The above distributions can be rescaled by the circumference of the circle as represented in the figure 5:

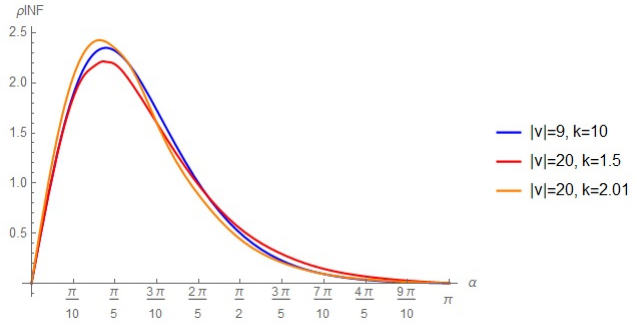

Figure 23: The figure 22 scaled with $2 \cdot \pi \cdot \sin(\alpha) \cdot \texttt{vacR}$

With given experimental measurement $\rho_\infty \texttt{Fin}(0)$ larger then in above example (eq. larger $|v|$ or k), the differences between the corresponding combinations of $|v|$ and k are further reduced. For even larger $\rho\texttt{Fin}(0)$, the contour lines corresponding to $\rho\texttt{Fin}(0)$ and $\rho\texttt{Fin}(\frac{\pi}{5})$ begin to overlap each other; the distribution is therefore uniquely determined by $\rho\texttt{Fin}(0)$. $|v|$ and k can be given only as a function $|v|(k)$.

8.3 Summary: Computability of $|v|$ and k

The results can be expanded to $|v| \in (0, 200]$ and $k \in (0, 200]$ by limiting the cell-space to a cone-like region as represented in figure 9.

Summarizing the above, with the experimental result ${}^e\rho_\infty$ given, we can approximately partition this area to: 13cm

1. The region A, where ${}^e\rho_\infty(0)$ uniquely determines the distribution and the parameters can be only given as a function $|v|(k)$.

2. The region B, where $|v|$ and k can be uniquely determined from ${}^e\rho_\infty(0)$ and a further value ${}^e\rho_\infty(\overline{\alpha})$, where $\overline{\alpha}$ should be chosen as described in section 8.2.2.

   The searched parameters will be obtained by computing ${}^0|v|(k)$ and ${}^\alpha|v|(k)$; then there are unique $|v|$ and k such that $|v| = {}^0|v|(k) = {}^\alpha|v|(k)$.

3. The region C of high $|v|$ and low k. The section 6 proves that the corresponding distributions converge to the case where the cargo comes straight to the vacuole and glides along it; here ρ_∞ can't be approximated by $\rho\texttt{Fin}$ due to numerical instabilities.

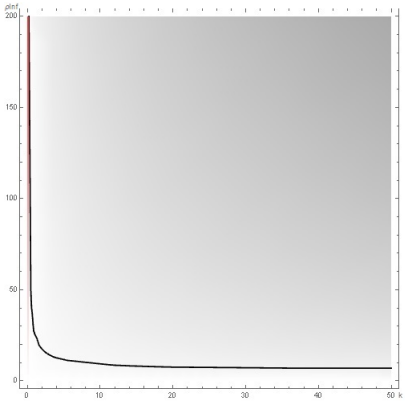

Figure 24: Contour line of ${}^e\rho_\infty(0)$ corresponding to $|v| = 9$ and $k = 10$. A corresponds approx. to the gray area, B to the white area below and left and C to the red strip at $k \approx 0$

8.4 Nonsymmetric Spatial Arrangement

If the vacuole is positioned nonysimmetrically to the line l (as defined in the section 5.5.3), then each of the halfcircles will be differently affected by the diffusive motion.

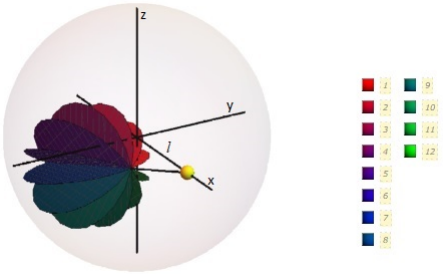

Figure 25: The center of the vacuole, `vacC`, placed in $-(\sqrt[3]{0.4}, \sqrt[3]{0.4}, \sqrt[3]{0.4})$; the nearest point is in the previous sections 0.2 away from the vacuole.

The advective component of motion is not affected by this, as it is never directed towards the cell membrane; therefore ρ`Fin` differs most between the halfcircles if $|v| = 0$.

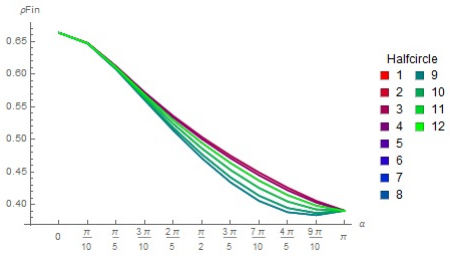

Figure 26: ρ`Fin` along the halfcircles in the figure 25 for $|v|$=0 and $k = 1$.

As expected, the differences vanish for large $|v|$:

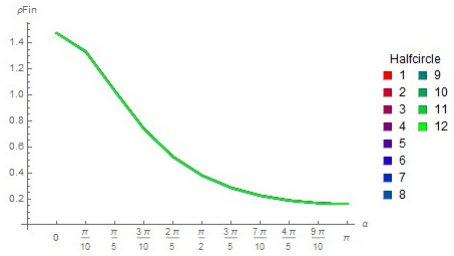

Figure 27: ρ`Fin` along the halfcircles for $|v|$=10 and $k = 1$.

To quantify this phenomenon for different $|v|$ and k, define

$$d(|v|, k) = \max_{\alpha\in[0,\pi],\ i,j\in\{1,\dots,12\}} \left| {}^{i}_{|v|,k}\rho\texttt{Fin}(\alpha) - {}^{j}_{|v|,k}\rho\texttt{Fin}(\alpha)\right|, \tag{85}$$

where ${}^{i}_{|v|,k}\rho\texttt{Fin}(\alpha)$ is the final cargo distribution along the halfcircle i on the vacuole.

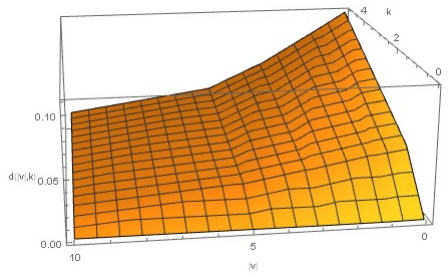

Figure 28: The value of $d(|v|, k)$

8.5 The Distance from Initial Position to the Vacuole

If the initial position of the cargo is closer to the vacuole, then the diffusion will act in much more limited space. The differences are most visible in the case of no advection; therefore assume first $|v| = 0$:

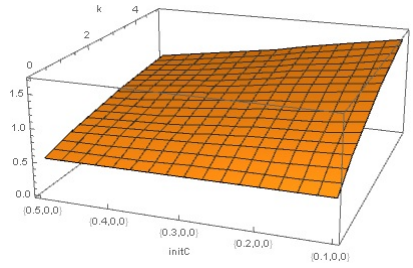

Figure 29: The value of $\rho\texttt{Fin}(0)$ depending on the choice of k and `initC`.

To get an insight whether the choice of different `initC` can contribute to distinguishability of broader range of $|v|$ and k, the contour lines conserving $\rho\texttt{Fin}(0)$ corresponding to $\texttt{initC} = (0.7, 0, 0)$ will be compared with those corresponding to $\texttt{initC} = (0.2, 0, 0)$:

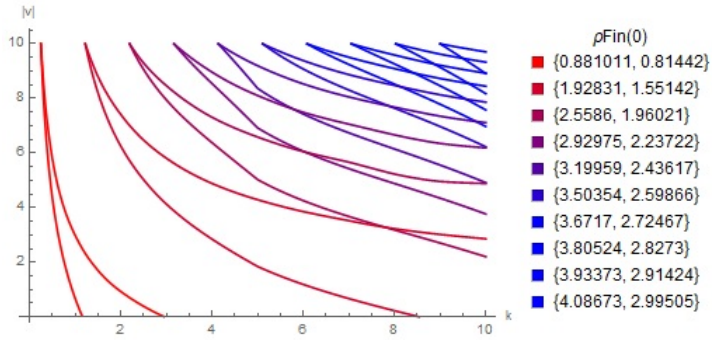

Figure 30: In each pair of the same color, the upper line corresponds to $\texttt{initC} = (0.7, 0, 0)$ and the lower line to $\texttt{initC} = (0.2, 0, 0)$

Analogously as in the section 8.2.3, these results suggest that comparing two distinct choices of `initC` allows to uniquely determine $|v|$ and k.

9 Conclusions

Investigation of a single case of the arrangement of the cell interior allows to determine the parameters $|v|$ and k in cases where the diffusion plays a sizable role in the motion of the cargo. From the obtained $|v|$ and k a distribution $\rho\texttt{Fin}$ can be calculated corresponding to an arrangement with different initial cargo position. Moreover, the size of the parameter d can be predicted for the case of nonsymmetric spatial arrangement. Both can be used as hypotheses and verified or refuted in additional experiments.

On the contrary, if the experimentally measured ${}^e\rho_\infty(0)$ is large, then $|v|$ and k can not be computed from a single case. Moreover, this case coincides with strong advection, therefore choosing an alternative initial cargo position won't bring much new information. Still, the absence of diffusion can be verified or refuted in separated experiment involving nonsymmetric spatial arrangement.

The case of very large $|v|$ and k or $|v|, k \to \infty$ describes a biologically different type of motion, as the cargo stays almost attached to the vacuolar membrane. The model connects it smoothly with the cases of smaller $|v|$ and k, however this is less useful as conducting numerical approximations is less eligible for large parameters. This case can not be distinguished from the one of smaller $|v|$ and k from a single distribution ${}^e\rho_\infty$ alone. However, as the diffusion is (almost) nonpresent away from the vacuole, the distinction is possible with an additional experiment involving nonsymmetric spatial arrangement if ${}^e\rho_\infty(0)$ is small enough.

References

[1] Iryna Monastyrska, Ester Rieter, Daniel J. Klionsky and Fulvio Reggiori, *Multiple roles of the cytoskeleton in autophagy*, August 2009, www.ncbi.nlm.nih.gov/pmc/articles/PMC2831541

[2] Danielle Glick, Sandra Barth and Kay F. Macleod, *Autophagy: cellular and molecular mechanisms*, May 2010, www.ncbi.nlm.nih.gov/pmc/articles/PMC2990190

[3] Fulvio Reggiori, Iryna Monastyrska, Takahiro Shintani and Daniel J. Klionsky, *The Actin Cytoskeleton Is Required for Selective Types of Autophagy, but Not Nonspecific Autophagy, in the Yeast* Molecular Biology of the Cell, Vol. 16, 5843-5856, December 2005

[4] Ephraim Fass, Elena Shvets, Ilan Degan, Koret Hirschberg and Zvulun Elazar, *Microtubules Support Production of Starvation-induced Autophagosomes but Not Their Targeting and Fusion with Lysosomes*, November 24, 2006 The Journal of Biological Chemistry, vol. 281, no. 47,pp. 36303-36316, www.jbc.org/content/281/47/36303.full.pdf

[5] *Simple diagram of yeast cell*, Wikimedia Commons, commons.wikimedia.org/wiki/File%3ASimple_diagram_of_yeast_cell_(numbers).svg

[6] *Motility of Kinesin*, commons.wikimedia.org/wiki/File%3AMotility_of_kinesin_en.png

[7] *Biologie-Skript zum MedAt 2017*, medat.oehmedwien.at/wp-content/uploads/sites/5/2015/04/BIO_2017ausgebessert.pdf

[8] *Biologie-Glossar*, http://www.biologie-online.eu/glossar

[9] *Principles of Mathematical Modeling*, second Edition, 2004, Elsevier Inc.

[10] *Science Daily, Reference Terms, Mathematical Model*, www.sciencedaily.com/terms/mathematical_model.htm

[11] Christian Schmeiser, *Lecture Notes for Mathematical Cell Biology* homepage.univie.ac.at/christian.schmeiser/MCB-skriptum.pdf

[12] Andreas Uttenweiler, Heinz Schwarz, Heinz Neumann and Andreas Mayer *The Vacuolar Transporter Chaperone (VTC) Complex is Required for Microautophagy* www.molbiolcell.org/content/early/2006/11/01/mbc.E06-08-0664.full.pdf

[13] Akira Okubo, Simon A. Levin *Diffusion and Ecological Problems: Modern Perspectives* Second Edtition, 2001, Springer-Verlag New York

Appendix

Here the most important parts of the mathematica-code are presented:

```
cellR = 1; (*Raius of the cell*)
vacC = {-0.4, 0, 0}; (the center of the vacuole *)
vacR = 0.4; (*radius of the vacuole*)
initC = {0.7, 0, 0}; (*expected value of the initial position of the cargo*)
α = (1 / Sqrt[(x - vacC[[1]])^2 + (y - vacC[[2]])^2 + (z - vacC[[3]])^2]) * (vacC - {x, y, z});
(*vectorfield of vectors directed to the center of the vacule*)
Needs["NDSolve`FEM`"]
(*The function generates a mesh over Ω - the mesh is denser in the area around the vacuole*)
genMesh[cellR_, initC_, vacC_, vacR_] :=
 Module[{cellMembrane, vacuole2, vacuole, initialPos, cellMembraneEL, vacuole2EL, vacuoleEL,
   initialPosEL, boundaryMesh},

  cellMembrane = ToBoundaryMesh[Sphere[{0, 0, 0}, cellR]];
  vacuole2 = ToBoundaryMesh[RegionIntersection[Ball[vacC, vacR + 0.3], Ball[{0, 0, 0}, cellR - 0.01]]];
  initialPos = ToBoundaryMesh[Sphere[{initC[[1]], initC[[2]], initC[[3]]}, 0.2]];
  vacuole = ToBoundaryMesh[Sphere[{vacC[[1]], vacC[[2]], vacC[[3]]}, vacR]];

  cellMembraneEL = cellMembrane["BoundaryElements"];
  vacuole2EL = vacuole2["BoundaryElements"];
  initialPosEL = initialPos["BoundaryElements"];
  vacuoleEL = vacuole["BoundaryElements"];
boundaryMesh =
   ToBoundaryMesh["Coordinates" → Join[cellMembrane["Coordinates"], vacuole2["Coordinates"],
      vacuole["Coordinates"]],
    "BoundaryElements" →
     Join[cellMembraneEL, MapThread[#1[#2] &,
       {Head /@ vacuole2EL, Length[cellMembrane["Coordinates"]] + ElementIncidents[vacuole2EL]}],
      MapThread[#1[#2] &, {Head /@ vacuoleEL, Length[cellMembrane["Coordinates"]] +
         Length[vacuole2["Coordinates"]] (*+Length[initialPos["Coordinates"]]*) +
         ElementIncidents[vacuoleEL]}]], "RegionHoles" → {{0, 0, 0}}];
ToElementMesh[boundaryMesh, "RegionMarker" → {{vacC + {vacR + 0.1, 0, 0}, 3, 0.05}},
   "RegionHoles" → {{vacC[[1]], vacC[[2]], vacC[[3]]}}, MeshQualityGoal → 1]]
genMesh[cellR, initC, vacC, vacR]["Wireframe"]
```

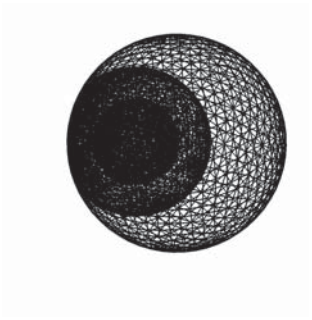

```
(*The function generates a mesh over Ω - the mesh has a triangular form covering only a part of Ω*)
minM = 0.0000008;
maxM = 0.00005;
genMesh[cellR_, initC_, vacC_, vacR_] :=
 Module[{Ω1, Ω2, boundMesh2, bElem2, boundaryMesh, envCone, boundEnv, bElemEnv},
  regA = ImplicitRegion[(x - vacC[[1]])^2 + (y - vacC[[2]])^2 + (z - vacC[[3]])^2 ≤ vacR^2 &&
     x > Cos[Pi/4] * vacR + 0.01, {x, y, z}];
  cone1 = Cone[{vacC + {Cos[Pi/4] * vacR, 0, 0}, initC + {0.25, 0, 0}}, Sin[Pi/4] * vacR];
  Ω1 = RegionDifference[cone1, regA];
  Ω2 = ImplicitRegion[(x - vacC[[1]])^2 + (y - vacC[[2]])^2 + (z - vacC[[3]])^2 ≤ vacR^2 &&
     x > vacC[[1]] + Cos[Pi/4] * vacR + 0.01, {x, y, z}];

boundMesh2 = ToBoundaryMesh[Ω2, MaxCellMeasure → minM];
```

```
  boundEnv = ToBoundaryMesh[cone1, MaxCellMeasure → maxM];

bElem2 = boundMesh2["BoundaryElements"];
  bElemEnv = boundEnv["BoundaryElements"];
  boundaryMesh = ToBoundaryMesh["Coordinates" → Join[boundMesh2["Coordinates"], boundEnv["Coordinates"]],
    "BoundaryElements" →
     Join[bElem2, MapThread[#1[#2] &,
       {Head /@ bElemEnv, Length[boundMesh2["Coordinates"]] + ElementIncidents[bElemEnv]}]]];
ToElementMesh[boundaryMesh, "RegionHoles" → {vacC + {vacR - 0.02, 0, 0}},
   MeshRefinementFunction → Function[{vertices, area}, Block[{x, y, z}, {x, y, z} = Mean[vertices];
      If[(x - vacC[[1]])^2 + (y - vacC[[2]])^2 + (z - vacC[[3]])^2 ≤ (vacR + 0.05)^2, area > minM,
       area > maxM]]]]

genMesh[cellR, initC, vacC, vacR]["Wireframe"]
```

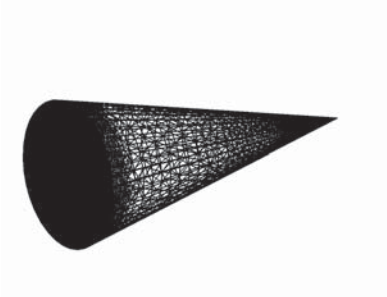

```
(*The main advection-diffusion equation*)
fSol[α_, k_, cellR_, vacC_, vacR_, initC_, vl_] :=
 Module[{Ω, mesh, c, initf, op, Γ},
  Ω = RegionDifference[Ball[{0, 0, 0}, cellR], Ball[{vacC[[1]], vacC[[2]], vacC[[3]]}, vacR]];
  mesh = genMesh[cellR, initC, vacC, vacR];
  (*generire die Dichte am Anfang, Integral über Ω soll 1 sein*)
  c =
   NIntegrate[
    PDF[MultinormalDistribution[{initC[[1]], initC[[2]], initC[[3]]},
        {{0.02, 0, 0}, {0, 0.02, 0}, {0, 0, 0.02}}], {#1, #2, #3} &[xN, yN, zN], {xN, yN, zN} ∈ Ω];
  initf[x_, y_, z_] :=
   (1 / c) * PDF[MultinormalDistribution[{initC[[1]], initC[[2]], initC[[3]]},
      {{0.02, 0, 0}, {0, 0.02, 0}, {0, 0, 0.02}}], {x, y, z}];

op =
   Inactive[Div][-{{1, 0, 0}, {0, 1, 0}, {0, 0, 1}}.Inactive[Grad][u[t, x, y, z], {x, y, z}] -
     Inactive[Times][vl * α, u[t, x, y, z]], {x, y, z}] + D[u[t, x, y, z], t];
  Γ = NeumannValue[-k * u[t, x, y, z], (x - vacC[[1]])^2 + (y - vacC[[2]])^2 + (z - vacC[[3]])^2 == vacR^2];
  NDSolveValue[{op == Γ, u[0, x, y, z] == initf[x, y, z]}, u, {t, 0, 20000}, {x, y, z} ∈ mesh]]

(*Function which generates testpoints along the halfcircles through the vacuole*)
genTestPoints[vacC_, vacR_, numP_] :=
 Module[{TestPoints, TestPoints3D, transF, rotationTable, TestPointsSphere, TestPointsVacuole0},
TestPoints = Drop[CirclePoints[{1, 0}, numP], -(numP / 2 - 1)];
  TestPoints3D = MapThread[Append, {TestPoints, ConstantArray[0, numP / 2 + 1]}];
(*rotate the test array x from z==0 by alpha*)
  transF[x_, α_] := {x[[1]], Cos[α] * x[[2]], Sin[α] * x[[2]]};
(*define Matrix TestPoints3D<>all angles*)
rotationTable = Table[{TestPoints3D[[j]], Pi * i/6}, {i, 0, 11}, {j, 1, numP / 2 + 1}];
(*generates the coordinates of all test points on the sphere*)
  TestPointsSphere = Apply[transF, rotationTable, {2}];
(*Rotate the TestPointsSphere so that it will show towards {0,0,0}
   (or towards the inital position of the particle)*)
TestPointsVacuole0 := Map[RotationTransform[{{1, 0, 0}, initC - vacC}], TestPointsSphere, {2}] ;
(*Resize the TestPointsSphere to the size of Vacuole and move it to appropriate condition*)
Map[# * vacR + vacC &, TestPointsVacuole0, {2}]]

(*Computation of ρInf. Only an example for the case k=0.5 and |v|=vl=1 is shown.*)
Do[Do[ufun = fSol[α, k, cellR, vacC, vacR, initC, vl];
g[m_] := NIntegrate[ufun[t, m[[1]], m[[2]], m[[3]]], {t, 0, 10000}];
  (*Here the integral will be computed on the following 29 points:*)
  joinedTestPoints = Join[Drop[genTestPoints[vacC, vacR, 200][[1]], -81],
    Drop[genTestPoints[vacC, vacR, 20][[1]], 2]];
```

```
  resPoints = Map[g, joinedTestPoints, {1}];
  Print[
   k * NIntegrate[ufun[t, x, y, z], {t, 0, 10000},
     {x, y, z} ∈ Sphere[{vacC[[1]], vacC[[2]], vacC[[3]]}, vacR]]];
  Ω = RegionDifference[Ball[{0, 0, 0}, cellR], Ball[vacC, vacR]];
  resPoints = k * resPoints;
intrF = ListInterpolation[resPoints, {Join[Array[# &, 20], Array[11 + # * 10 &, 9]]}, Method → "Spline"];
Print[Plot[intrF[x], {x, 1, 101}, PlotRange → Full]];
  (*Integral of the interpolated result over the vacuole*)
  Print[
   {NIntegrate[2 * Pi * y * intrF[(100/Pi) * ArcSin[y / vacR] + 1],
     {x, y} ∈ ImplicitRegion[0 ≤ x && 0 ≤ y && x^2 + y^2 == vacR^2, {x, y}]] +
    NIntegrate[2 * Pi * y * intrF[(100/Pi) * (Pi - ArcSin[y / vacR]) + 1],
     {x, y} ∈ ImplicitRegion[x ≤ 0 && 0 ≤ y && x^2 + y^2 == vacR^2, {x, y}]], "vl", vl, "k", k}];
Save["D:\\results_neu\\20_3_vl" <> ToString[vl] <> "_k" <> ToString[k * 100], resPoints], {k, {0.5}}],
 {vl, {1}}]
1.001741209747205`
```

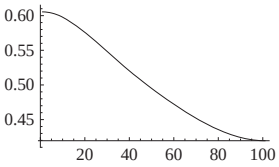


```
{1.0017298469727411`, "vl", 1, "k", 0.5`}
(*The following code computes the countor lines of ρInf:*)
maxK = 20;
maxV = 50;

kVlValue0 = kVlValue;
kVlValue0 = Interpolation[kVlValue0];
stopF[u_] := Max[0.01, FindRoot[(kVlValue0[#, maxV] - u) &[x], {x, 0}][[1]][[2]]] ;
(*finds k, where the graph falls bellow u*)
kPoints[u_] := Array[# &, 100, {stopF[u], maxK}];
findV[u_, k_] := FindRoot[kVlValue0[k, y] - u, {y, 0}];
vPoints[u_] := #[[1]][[2]] & /@ (findV[u, #] & /@ kPoints[u]);
pointsU[u_] := Transpose[{kPoints[u], vPoints[u]}];
kSamples = Array[# &, 13, {1, 20}];
uSamples = kVlValue0[#, maxV] & /@ kSamples;
(*uSamples=Array[#&,15,{0.1,maxU}]*)
str = pointsU /@ uSamples;
toPlot = Select[#, #[[2]] ≥ 0 && #[[2]] ≤ maxV && #[[1]] ≥ 0.01 && #[[1]] ≤ maxK &] & /@ str;
toPlot = Select[toPlot, Length[#] > 0 &];
Print[ListLinePlot[toPlot, PlotRange → Full, PlotLegends → SwatchLegend[uSamples, LegendLabel → "ρFin(0)"],
    AxesLabel → {"k", "|v|"},
    PlotStyle → Join[Array[RGBColor[1 - #/6, 0, #/6] &, 6, 0], Array[RGBColor[0, #/6, 1 - #/6] &, 6]]]];
```

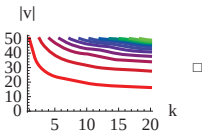


```
(*A function which computes the expression d(|v|,k) from the section 8.4 *)
difFct[resPoints_] := Module[{testP0, testP, difF, difR, minR, maxR},
  testP0 = #[9] & /@ Interpolation /@ resPoints;
testP = Transpose[{Array[# &, Length[testP0]], testP0}];
minR = MinimalBy[testP, #[[2]] &][[1]][[1]];
  maxR = MaximalBy[testP, #[[2]] &][[1]][[1]];
  difF[x_] := Interpolation[resPoints[[maxR]]][x] - Interpolation[resPoints[[minR]]][x];
  difR = FindMaximum[{difF[x], 1 ≤ x ≤ 11}, x][[1]]]
```